International Geology Review, Vol. 45, 2003, p. 898–921.

Jurassic Gabbro-Granite-Syenite Suites from Southern Jiangxi Province, SE China: Age, Origin, and Tectonic Significance

XIAN-HUA LI,[1] ZHIGANG CHEN,

Guangzhou Institute of Geochemistry, Chinese Academy of Sciences, Guangzhou 510640, China

DUNYI LIU,

Institute of Geology, Chinese Academy of Geological Science, Beijing 100037, China

AND WU-XIAN LI

Guangzhou Institute of Geochemistry, Chinese Academy of Sciences, Guangzhou 510640, China

Abstract

SHRIMP U-Pb zircon and hornblende $^{39}Ar/^{40}Ar$ ages, major and trace elements, and Sr-Nd isotopes are reported for the Chebu gabbro, the Zhaibei granite, and the Quannan and Tabei syenites, southern Jiangxi, Southeast China. Two major episodes of Jurassic magmatism were identified, i.e., the ~172 Ma bimodal gabbro-granite and the ~165 Ma syenite suites. The Chebu gabbros show geochemical affinities of intraplate transitional basaltic rocks with restricted Sr and Nd isotopic variations (I_{Sr} = 0.7065 to 0.7067, εNd(T) = +0.55 to –0.82). The Zhaibei granites have variable εNd(T) values (–0.78 to –6.55) and $I_{Sr} > 0.710$. They share geochemical characteristics with aluminous A_2-type granites, and probably were generated by shallow dehydration melting of hornblende-bearing granitoid source rocks heated by contemporaneous intrusion of mantle-derived basaltic magmas. The Quannan and Tabei syenites are high in K_2O, with K_2O/Na_2O ratios of 0.9–1.3, typical of shoshonitic affinities. They have a relatively large range of Sr and Nd isotopic compositions (I_{Sr} = 0.704–0.710, εNd(T) = –3.54 to +3.44). Among them, the least crust-contaminated syenites display OIB-type incompatible trace-element patterns with Nb/La >1 and Nb/Th >14. The geochemical and isotopic data of the gabbros and syenites imply that their mantle sources might have been metasomatized by OIB-type melts in an intraplate regime, contrasting with the subduction-related metasomatism occurring in the mantle wedge overlying a subduction zone. The 172–165 Ma gabbro-A-type granite-syenite suites in southern Jiangxi are coeval with the 175–160 Ma alkaline basalts and syenites in southern Hunan–southeastern Guangxi, suggesting that an extension-to-rifting regime was dominant over much of Southeast China during the Middle to Late Jurassic. This rifted continental margin seems appropriate to account for the widespread Middle to Late Jurassic magmatism in Southeast China.

Introduction

THE MESOZOIC GEOLOGY of Southeast China is characterized by intensive, widespread magmatism (Fig. 1). Among the igneous rocks formed, granites and rhyolites are volumetrically dominant, with subordinate gabbros and basalts, and rare intermediate lithologies. Although late Mesozoic granitoids and volcanic rocks are confined mostly to coastal areas, early Mesozoic intrusions occur mainly in the interior. As a major part of East Asia, Southeast China is a very complex region involving multiple stages of Mesozoic tectono-magmatic activity. The problematic regime that accounted for Mesozoic magmatism in Southeast China has been an issue of little consensus. Various tectonic models have been proposed in the last two decades, which can be grouped generally into four categories: (1) an active continental margin related to the subduction of a paleo-Pacific plate (e.g., Jahn et al., 1976; Holloway, 1982; Huang et al., 1986; Zhou and Li, 2000); (2) an Alpine-type continental collision (Hsü et al., 1988, 1990); (3) a wrench fault system (Xu et al., 1987, 1993); and (4) continental extension and rifting (Gilder et al., 1991, 1996; Li, 2000).

Relative to numerous studies of late Mesozoic magmatism in the coastal areas, less attention has been paid to the vast early Mesozoic magmatism in

Corresponding author; email: lixh@gig.ac.cn

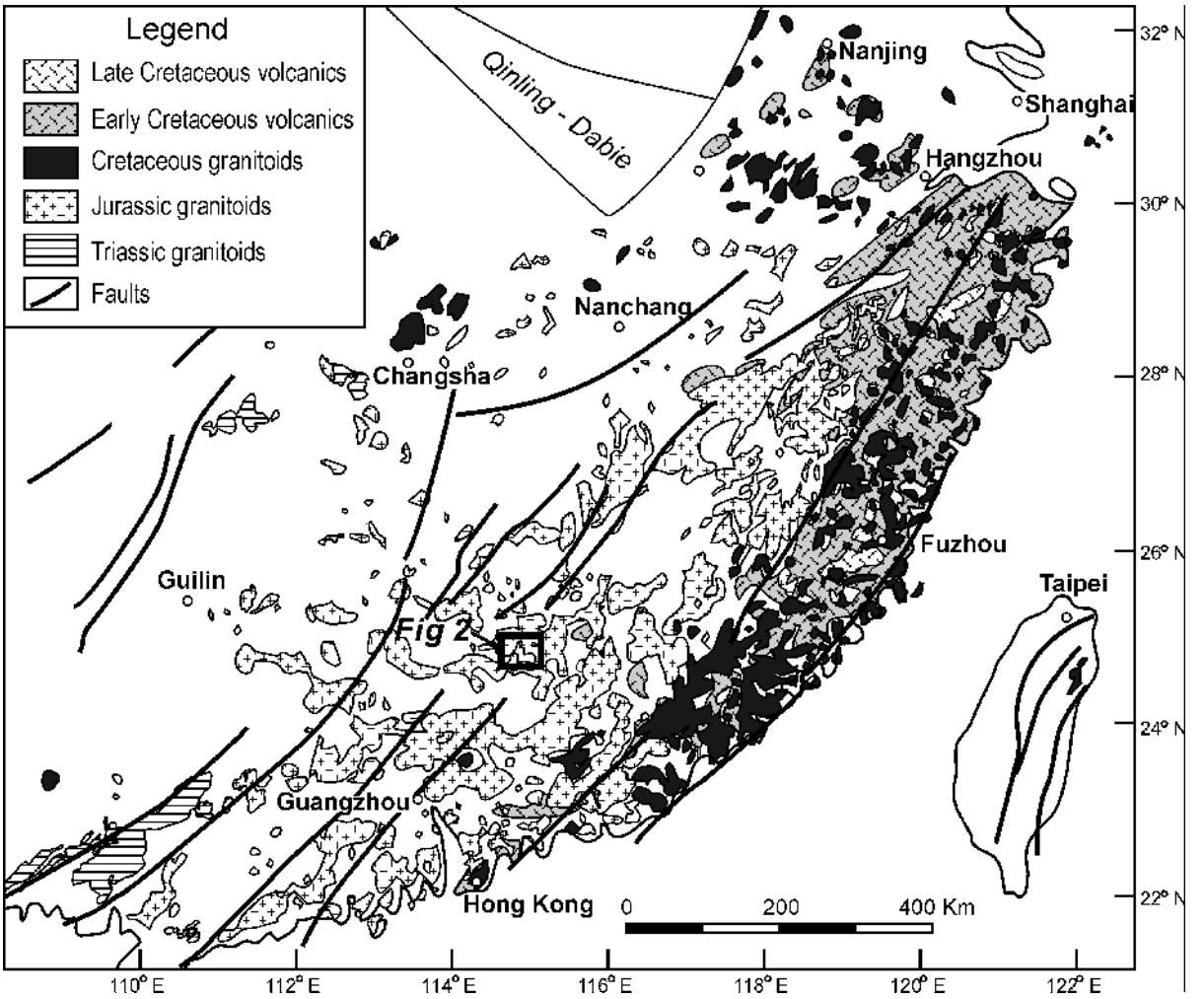

FIG. 1. Distribution of Mesozoic igneous rocks in Southeast China.

Southeast China's interior. We have conducted a comprehensive study of SHRIMP U-Pb zircon and hornblende $^{39}Ar/^{40}Ar$ dating, geochemical and Sr-Nd isotopes for the gabbro-granite–syenite suites from southern Jiangxi Province. These new data were used to explore the petrogenesis and shed new light on the Mesozoic tectonics of Southeast China.

Geological Background

Southern Jiangxi includes the central part of the early Mesozoic magmatic belt of the interior of Southeast China (Fig. 1). Sinian to Ordovician flysch sequences comprise the basement that was tightly folded and metamorphosed to greenschist facies. The basement was intruded by Caledonian-age granitoids and is overlain unconformably by Upper Devonian to Lower Triassic shallow-marine carbonates, clastic deposits, and flysch sedimentation (JBGMR, 1989). Mesozoic volcano-sedimentary basins developed since Jurassic time, with volcanic rocks up to 800 m in thickness uncomfortably overlying the pre-Jurassic strata. The volcanic rocks consist of bimodal basalts and rhyolites dated at 163–179 Ma by Rb-Sr whole-rock analysis (Chen et al., 1999).

Mesozoic granite intrusions are dominant in the study area, including the Pitou pluton to the northwest, the Keshubei plutons to the northeast, and the Zhaibei pluton to the east (Fig. 2). They intrude the Paleozoic strata and granitoids. Rb-Sr isochron dates of 176 Ma and 178 Ma were reported for the Zhaibei and Pitou granites, respectively, by Chen et al. (1999) and Fan and Chen (2000). The Chebu gabbro, a few small intrusions with an outcrop area of ~20 km^2, intruded exclusively within the Zhaibei

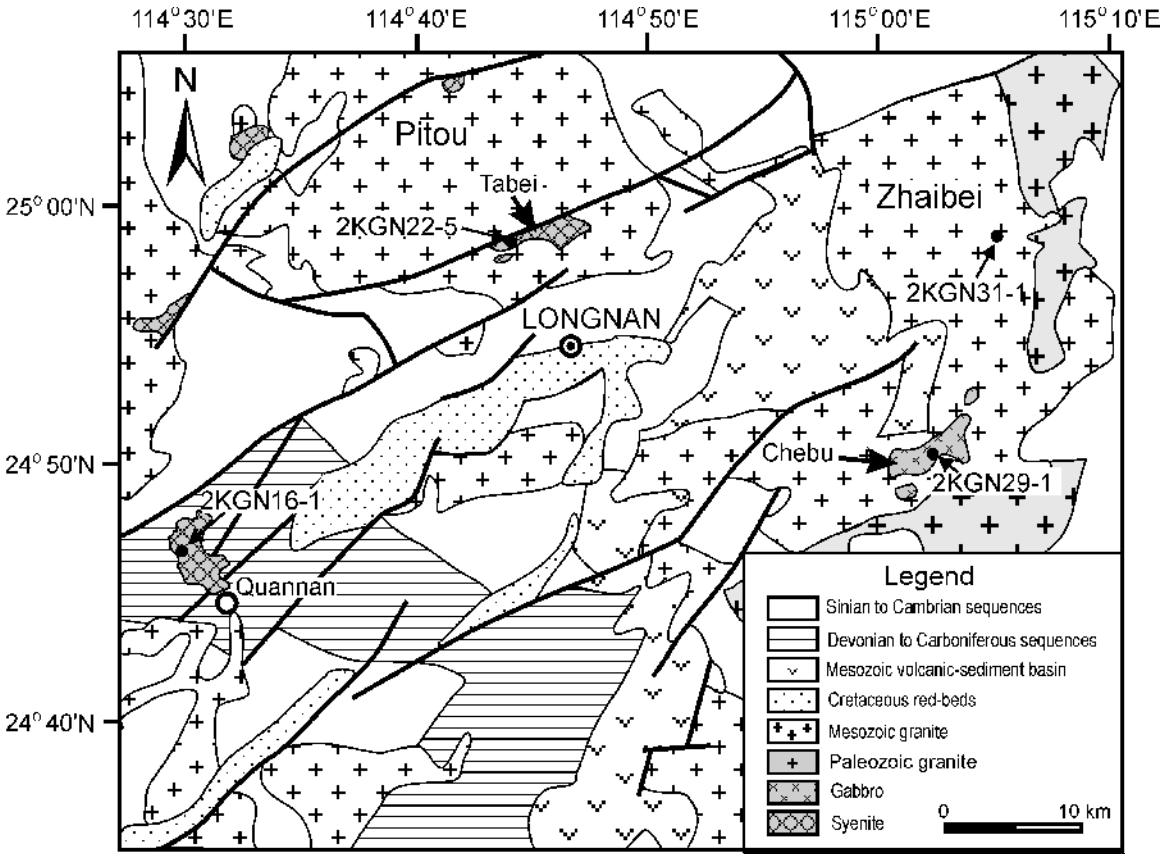

FIG. 2. Geological sketch map of southern Jiangxi (modified after JBGMR, 1989). Sample locations are indicated.

granite. The contact between the Chebu gabbro and the Zhaibei granite is lobate to crenulate shaped. A zone of magma mingling a few meters to several tens of meters in width contains abundant gabbroic enclaves from 10 cm to 5 m in size. Most gabbro enclaves are rounded, subrounded to elongated, and only a few are irregular in shape. On the other hand, granitic veins also occur within the gabbro near the contact zone. These veins, generally irregular in shape with compositions similar to the Zhaibei granite, were described as back-veins by Vernon et al. (1988). These field observations suggest that the Chebu gabbro intruded the Zhaibei granite when they both were in semi-solid states.

In addition to the granite and gabbro intrusions, a few small syenite intrusions occur in the study area. They intrude Paleozoic strata and the Pitou granite; a syenite pluton is unconformably overlain by Lower Cretaceous redbeds. In this study, we report the results of chronological, geochemical, and Sr-Nd isotopic analyses of the Chebu gabbro, the Zhaibei granite, and the Quannan and Tabei syenites, and discuss their origin and tectonic implications for the Jurassic of Southeast China.

Petrography

The Chebu gabbro is coarse- to medium-grained, containing 40–50% plagioclase, 20–30% hornblende, 10–20% pyroxene, 2–5% biotite, and trace amounts of zircon, apatite, magnetite, and ilmenite. The hornblende is altered and partially replaced by biotite and muscovite. Some plagioclase crystals show a two-generation growth: a calcic plagioclase mantle (An $\approx$ 60) and an overgrowth sodic plagioclase rim (An = 28–30). The formation of such two-generation, discordant plagioclases may be indicative of magma mingling (Xu et al., 1999); i.e., the calcic plagioclase cores crystallized in a hotter gabbroic magma in the early stage, and then the overgrowth rims formed at the late stage as a result of solid-liquid disequilibrium when the gabbroic magma mingled with a relatively cooler, lower-Ca felsic magma.

The Zhaibei granite is pink, coarse-grained in the inner zone, and fine-grained to porphyritic in the marginal zone. It contains 40–50% K-feldspar, 40–50% quartz, with minor amounts of plagioclase and biotite. Accessory minerals include zircon, apatite, magnetite, allanite and monazite. Biotite is altered to varying degrees by chloritization.

The Quannan syenite is an alkaline complex, including aegirine syenite, quartz syenite, and porphyritic quartz monzonite. The aegirine syenite is coarse- to medium-grained, containing ~90% K-feldspar, <5% aegirine, <5% quartz, and a minor amount of diopside, zircon, apatite, and magnetite. The quartz syenite, also coarse- to medium-grained, is composed of 85–90% K-feldspar, 5–10% quartz, 2–5% hornblende, and minor amounts of zircon, apatite, titanite, and magnetite. Hornblende is heavily chloritized.

The minor porphyritic quartz monzonite contains ~50% phenocryst minerals including 15–20% K-feldspar, 5–10% quartz, 10–15% plagioclase (An = ~30), and 10–15% hornblende. The fine-grained matrix is composed mainly of K-feldspar, quartz, and plagioclase. Hornblende phenocrysts were severely altered by chloritization. The Tabei syenite is porphyritic, containing 20–30% K-feldspar phenocrysts and fine-grained, matrix minerals including 40–50% K-feldspar, 15–20% alkali amphibole and 5–10% quartz. Accessory minerals are zircon, apatite, and magnetite. The alkali amphibole is anhedral and interstitial, suggesting it crystallized at a late stage of rock formation.

Analytical Procedures

Samples for U-Pb analysis were processed by conventional magnetic and gravitational techniques to concentrate non-magnetic, heavy fractions. A representative selection of zircons was extracted from each concentrate by hand-picking under a binocular microscope. Zircon grains, together with a zircon U-Pb standard, were mounted in epoxy, which was then polished to section the crystals for analysis. Zircons were investigated using transmitted and reflected light micrographs and backscattered electron (BSE) images, and the mount was vacuum-coated with a 500 nm layer of high-purity gold. Measurements of U, Th, and Pb (Table 1) were conducted using the SHRIMP II ion microprobe at the Institute of Geology, Chinese Academy of Geological Sciences, Beijing. U-Th-Pb ratios were determined relative to the TEMORA standard zircon ($^{206}Pb/^{238}U$ = 0.0668 corresponding to 417 Ma), analyses of which were interspersed with those of unknown grains, using operating and data processing procedures similar to those described by Williams (1998) and Song et al. (2002). The mass resolution used to measure Pb/Pb and Pb/U isotopic ratios was ~5000 during the analyses. Measured compositions were corrected for common Pb by assuming $^{206}Pb/^{238}U$–$^{208}Pb/^{232}Th$ age concordance. Corrections are sufficiently small to be insensitive to the choice of common Pb composition, and an average crustal composition (Cumming and Richards, 1975) appropriate to the age of the mineral was assumed. Uncertainties on individual analyses are reported at the 1σ level; mean ages for pooled $^{206}Pb/^{238}U$ analyses are quoted with a 95% confidence interval, except where noted otherwise, including uncertainty in calibration against the TEMORA zircon standard.

A hornblende separate extracted from the Tabei syenite was wrapped in an aluminum foil packet, stacked in an aluminum canister along with the LP-6 Biotite standard (Odin et al. 1982) and then irradiated for 30 hours in the VT-C position at the THOR Reactor in Taiwan. After irradiation, standard and sample were degassed incrementally from 400 to 1200ºC, following a 30 minute/step schedule, using a resistance furnace. The purified gas was analyzed with a Varian-MAT GD150 mass spectrometer at the Department of Geosciences, National Taiwan University, following procedures outlined in detail by Lo and Lee (1994). The mean of J-values obtained from the monitor standard was adopted in age calculation. The $^{40}Ar/^{39}Ar$ analytical result is listed in Table 2.

Major-element oxides were determined using a Varian Vista PRO ICP-AES at the Guangzhou Institute of Geochemistry, Chinese Academy of Sciences. The details of the analytical procedures were described by Li et al. (2002a), with sample powders being fused with lithium metaborate at ~1100ºC. Analytical precision is better than 2%. Trace elements were analyzed using a Perkin-Elmer Sciex ELAN 6000 ICP-MS at the Guangzhou Institute of Geochemistry. About 50 mg sample powders were dissolved in high-pressure Teflon bombs using a HF + HNO_3 mixture. An internal standard solution containing the single element Rh was used to monitor signal drift during ion counting. The USGS standards BCR-1, W-2, and G-2, and the Chinese National standards GSR-1 and GSR-3, were chosen for calibrating element concentrations of measured samples. In-run analytical precision for most elements was generally better than 2–5%. Detailed

TABLE 1. SHRIMP U-Pb Zircon Data

Anal. #	U (ppm)	Th (ppm)	Th/U	f_{206}[1] (%)	$^{207}Pb^*/^{235}U$ (± %error 1σ)		$^{206}Pb^*/^{238}U$ (± %error 1σ)		206/238 age (Ma) (±1σ)	
Chebu Gabbro, 2KGN29-1 (24°50'30.2"N, 115°02'10.3"E)										
1-1	1239	1035	0.86	1.10	0.1664	3.1	0.02807	2.7	178.5	±5.7
2-1	4118	5906	1.48	0.86	0.1709	2.7	0.02876	2.6	182.8	±6.4
3-1	2245	2408	1.11	0.52	0.1933	2.8	0.02968	2.7	188.5	±6.1
4-1	1520	1542	1.05	0.41	0.1849	2.9	0.02682	2.6	170.6	±5.4
5-1	1480	1473	1.03	1.33	0.1619	3.0	0.02720	2.7	173.0	±5.6
6-1	416	380	0.94	1.76	0.1731	3.6	0.02713	2.7	172.5	±5.5
7-1	4318	3196	0.76	0.36	0.1756	2.7	0.02708	2.6	172.2	±5.1
8-1	2007	2886	1.49	0.58	0.1636	3.0	0.02582	2.6	164.3	±5.7
9-1	4409	3673	0.86	0.00	0.1786	2.8	0.02523	2.7	160.7	±5.0
10-1	2396	2614	1.13	0.53	0.1745	2.9	0.02798	2.7	177.9	±5.9
11-1	1591	1886	1.23	0.22	0.1911	2.9	0.02768	2.6	176.0	±5.7
12-1	3032	3393	1.16	0.15	0.1754	2.8	0.02600	2.6	165.5	±5.3
13-1	3020	1034	0.35	2.44	0.2460	7.2	0.03287	2.8	208.5	±6.3
14-1	1333	1354	1.05	0.30	0.1837	2.9	0.02672	2.6	170.0	±5.4
Zhaibei granite, 2KGN31-1 (24°58'43.4"N, 115°05'09.9"E)										
1-1	748	631	0.87	1.12	0.1842	3.1	0.02888	2.7	183.5	±5.7
2-1	1360	1062	0.81	0.54	0.1726	2.9	0.02756	2.6	175.3	±5.3
3-1	370	222	0.62	0.80	0.1878	4.0	0.02745	2.9	174.6	±5.6
4-1	1643	860	0.54	1.37	0.1889	2.9	0.03061	2.6	194.3	±5.6
5-1	694	605	0.90	3.43	0.1792	5.2	0.02812	2.7	178.8	±5.6
6-1	1971	882	0.46	0.38	0.1787	2.8	0.02633	2.6	167.5	±4.7
7-1	455	225	0.51	0.17	0.1803	3.4	0.02686	2.7	170.8	±4.9
8-1	395	197	0.52	1.87	0.1746	4.0	0.02597	2.7	165.3	±4.9
9-1	109	50	0.48	4.91	0.1900	5.9	0.02828	2.9	179.8	±5.8
10-1	433	241	0.58	1.15	0.1716	3.8	0.02550	2.8	162.3	±5.0
11-1	732	525	0.74	3.77	0.1798	4.0	0.02793	2.7	177.6	±5.4
12-1	562	321	0.59	9.83	0.1830	7.5	0.02889	2.7	183.6	±5.7
13-1	473	281	0.61	1.55	0.1649	3.7	0.02562	2.7	163.1	±4.9
14-1	373	216	0.60	3.03	0.1827	4.8	0.02642	2.7	168.1	±5.1
15-1	407	145	0.37	1.39	0.1851	3.6	0.02478	2.7	157.8	±4.5
Quannan syenite, 2KGN16-1 (24°46'20.4"N, 114°29'55.7"E)										
1-1	355	377	1.10	0.59	0.1683	3.8	0.02536	2.9	161.4	±5.7
2-1	324	297	0.95	0.75	0.1699	3.9	0.02604	2.8	165.7	±5.6
3-1	480	580	1.25	0.30	0.1806	3.3	0.02548	2.7	162.2	±5.4
4-1	489	636	1.34	0.33	0.1820	3.3	0.02643	2.7	168.2	±5.7
5-1	403	377	0.96	0.05	0.1907	3.4	0.02621	2.7	166.8	±5.2
6-1	347	390	1.16	0.70	0.1764	3.7	0.02621	2.8	166.8	±5.8
7-1	629	715	1.18	0.36	0.1773	3.5	0.02641	2.6	168.0	±5.5
8-1	561	309	0.57	0.38	0.1824	3.3	0.02689	2.7	171.0	±5.1
9-1	602	755	1.30	0.00	0.1960	3.2	0.02633	2.7	167.5	±5.6
10-1	523	516	1.02	0.53	0.1825	3.4	0.02717	2.7	172.8	±5.5
11-1	255	227	0.92	1.18	0.1544	4.8	0.02439	2.7	155.3	±5.1
12-1	618	360	0.60	0.33	0.1658	3.4	0.02560	2.8	162.9	±5.0
13-1	1635	852	0.54	0.09	0.1761	2.9	0.02531	2.7	161.2	±4.7
14-1	379	270	0.74	1.99	0.1411	4.2	0.02577	2.7	164.0	±5.1
15-1	311	252	0.84	0.56	0.1752	3.8	0.02537	2.7	161.5	±5.1

[1] f_{206} = percentage of common ^{206}Pb in total ^{206}Pb.

TABLE 2. ^{40}Ar-^{39}Ar Analytical Data for Hornblende from the Tabei Syenite (2KGN22-5, 24°57'59.1"N, 114°44'14.3"E)[1]

T (°C)	cum. ^{39}Ar	atoms. (%)	$^{36}Ar/^{39}Ar$	$^{37}Ar/^{39}Ar$	$^{38}Ar/^{39}Ar$	$^{40}Ar/^{39}Ar$	$^{40}Ar/^{36}Ar$	Date (Ma)±1σ	
800	0.027	34.21	8.24E-02	1.16E+00	7.21E-01	7.09E+01	8.61E+02	232.7	±21.5
900	0.041	28.82	3.10E-02	7.90E–01	1.33E-02	3.16E+01	1.02E+03	116.0	±6.4
950	0.052	7.80	9.31E-03	1.33E+00	1.73E-04	3.40E+01	3.65E+03	159.5	±2.5
975	0.065	2.79	3.52E-03	1.61E+00	1.51E-04	3.29E+01	9.36E+03	162.7	±4.1
1000	0.078	0.00	1.47E-04	1.70E+00	1.47E-04	3.15E+01	2.14E+05	160.1	±2.1
1050	0.129	8.15	9.86E-03	1.97E+00	6.87E-02	3.40E+01	3.45E+03	159.0	±0.8
1075	0.168	1.54	2.36E-03	2.51E+00	8.26E-02	3.30E+01	1.40E+04	165.1	±0.6
1100	0.220	2.68	3.50E-03	2.30E+00	9.34E-02	3.22E+01	9.18E+03	159.4	±0.3
1180	0.337	1.58	2.33E-03	2.37E+00	1.17E-01	3.23E+01	1.39E+04	161.8	±0.4
1250	0.476	2.11	3.01E-03	2.61E+00	1.31E-01	3.28E+01	1.09E+04	163.3	±0.3
1600	1.000	7.17	8.97E-03	3.74E+00	8.17E-01	3.31E+01	3.69E+03	156.6	±0.2

[1]Sample mass = 758.0 mg; J-value = 0.002950 ± 0.000003; integrated date of all stages = 160.6 ± 1.0 Ma (2).

procedures for trace element analysis by ICP-MS were described by Liu et al. (1996) and Li (1997). The analytical results of major and trace elements are listed in Tables 3 and 4.

Sr and Nd fractions were separated by passing through cation columns, and the Nd was further purified employing an HDEHP column. Sr and Nd isotopic compositions were determined using a Micromass Isoprobe multi-collector mass spectrometer (MC-ICPMS) operated in static mode at the Guangzhou Institute of Geochemistry. Measured $^{87}Sr/^{86}Sr$ and $^{143}Nd/^{144}Nd$ ratios were normalized to $^{86}Sr/^{88}Sr = 0.1194$ and $^{146}Nd/^{144}Nd = 0.7219$, respectively. Analytical procedures are similar to those described by Wei et al. (2002) and Liang et al. (2003). The reported $^{87}Sr/^{86}Sr$ and $^{143}Nd/^{144}Nd$ ratios were further adjusted relative to the NBS SRM 987 standard of 0.71025 and the Shin Etsu JNdi-1 standard of 0.512115, corresponding to the La Jolla standard of 0.511860 (Tanaka et al. 2000), respectively. Sr and Nd isotopic data are presented in Table 5.

Results

SHRIMP U-Pb zircon dates

The Chebu gabbro (sample 2KGN29-1, 24°50'30.2" N, 115°02'10.3" E). Zircons in this sample are mostly euhedral, up to 100 μm in length, and have length to width ratios mostly of 2:1. Most crystals are transparent and light brown in color. Euhedral concentric zoning is common in most crystals. Fourteen analyses of 14 zircons from this sample were obtained in sets of seven scans during a single analytical session. U concentrations are highly variable, ranging from 416 to 4409 ppm, and Th ranges from 380 to 5906 ppm. Th/U ratios vary mostly between 0.76 and 1.48, with the exception of analysis #13-1 that has a significantly lower Th/U ratio of 0.36 and an older $^{206}Pb/^{238}U$ age of 207 Ma than the main group, and is likely a xenocryst. The remaining 13 analyses form a single, concordant group with a weighted mean $^{206}Pb/^{238}U$ age of 172.9 ± 4.3 Ma (Fig. 3A, MSWD = 1.81), which gives the best estimate of the crystallization age of the Chebu gabbro.

The Zhaibei granite (sample 2KGN31-1, 24°58'43.4", 115°05'09.9" E). Zircons are euhedral, colorless and transparent, and up to ~150 μm in length, with length-to-width ratios up to 4:1. Euhedral concentric zoning is common in most crystals. Fifteen analyses were conducted of 15 zircons in sets of seven scans. Concentrations of U range from 109 to 1971 ppm, and Th from 50 to 1062 ppm. Th/U ratios vary between 0.37 and 0.90. All analyses but analysis #4-1, which deviates from the main

TABLE 3. Major and Trace Element Data for the Chebu Gabbro

Sample	2KGN29-1	2KGN29-2	2KGN29-4	2KGN29-5	2KGN29-6	2KGN29-9
			Major (%)			
SiO_2	48.81	50.12	50.69	51.33	49.63	50.89
TiO_2	1.32	1.46	1.26	1.17	1.47	1.37
Al_2O_3	16.22	16.60	15.65	16.06	16.80	16.31
Fe_2O_3	10.22	10.59	10.30	10.22	11.21	10.41
MnO	0.14	0.15	0.14	0.15	0.16	0.14
MgO	7.58	7.74	8.16	7.55	7.63	7.45
CaO	8.28	8.41	7.84	7.77	8.75	8.11
Na_2O	2.79	2.98	2.65	2.91	2.97	2.95
K_2O	1.38	1.01	1.17	1.05	0.85	1.13
P_2O_5	0.22	0.24	0.12	0.22	0.24	0.24
LOI	2.30	1.52	1.32	1.34	1.15	1.68
Total	99.26	100.80	99.32	99.78	100.87	100.67
Mg#	0.57	0.57	0.59	0.57	0.55	0.57
			Trace (ppm)			
Sc	19.8	21.6	18.6	17.7	22.6	20.7
V	146	157	135	127	164	151
Cr	73.1	69.4	70.1	53.8	73.4	61.9
Ni	127	127	141	125	98.3	128
Ga	18.6	18.9	17.9	19.2	18.7	19.0
Rb	65.1	41.3	58.7	52.5	33.5	48.1
Sr	267	278	264	263	283	263
Y	24.0	24.7	21.7	26.9	22.9	26.9
Zr	125	131	113	133	120	123
Nb	15.9	16.3	13.6	16.6	15.4	17.9
Cs	2.25	1.85	2.58	2.16	1.83	1.88
Ba	171	140	171	150	143	150
La	17.4	18.1	16.6	20.9	16.3	20.1
Ce	37.4	39.4	35.6	44.6	35.2	42.8
Pr	4.38	4.53	4.03	5.04	4.12	4.94
Nd	18.6	19.2	17.0	20.4	17.8	20.6
Sm	4.60	4.64	4.10	4.84	4.37	5.01
Eu	1.37	1.40	1.22	1.20	1.43	1.41
Gd	4.64	4.81	4.30	4.88	4.47	5.12
Tb	0.75	0.78	0.68	0.80	0.72	0.83
Dy	4.47	4.60	4.01	4.79	4.22	4.98
Ho	0.91	0.91	0.80	0.97	0.85	0.99
Er	2.52	2.65	2.26	2.72	2.41	2.80
Tm	0.36	0.37	0.32	0.40	0.35	0.41
Yb	2.27	2.32	2.00	2.48	2.17	2.51
Lu	0.35	0.35	0.30	0.36	0.34	0.37
Hf	3.65	3.76	3.23	3.80	3.34	3.53
Ta	1.16	1.23	0.96	1.18	1.09	1.32
Pb	6.97	5.77	6.54	7.80	5.51	6.55
Th	5.79	6.85	5.66	5.28	5.10	6.44
U	1.38	1.46	1.37	1.45	1.11	1.45

Mg# = $Mg/(Mg + Fe^{2+})$, assuming $Fe_2O_3/(FeO + Fe_2O_3) = 0.20$. Total iron as Fe_2O_3.

TABLE 4. Major and Trace Element Data for the Zhaibei Granite and the Quannan and Tabei Syenites

Sample	2KGN28-1	2KGN28-6	2KGN30-2	2KGN30-4	2KGN31-3	2KGN33-1	2KGN34-2	2KGN34-5	2KGN34-7
					Major (%)				
SiO_2	74.29	74.84	76.65	75.54	71.07	71.30	76.00	76.52	76.11
TiO_2	0.18	0.19	0.09	0.09	0.44	0.29	0.09	0.09	0.10
Al_2O_3	12.65	12.45	11.89	12.21	13.51	13.77	11.92	12.12	12.14
Fe_2O_3	2.37	1.88	1.63	1.60	3.72	2.73	1.67	2.06	1.83
MnO	0.03	0.02	0.02	0.02	0.05	0.02	0.02	0.01	0.03
MgO	0.17	0.27	0.04	0.04	0.45	0.24	0.05	0.10	0.06
CaO	0.78	0.80	0.47	0.50	1.10	0.98	0.55	0.15	0.55
Na_2O	3.66	2.65	3.12	3.20	2.97	3.20	2.91	2.50	3.04
K_2O	4.82	4.89	5.27	5.11	5.53	5.62	4.94	5.38	5.44
P_2O_5	0.10	0.04	0.01	0.01	0.08	0.05	0.00	0.02	0.02
LOI	0.95	1.50	0.81	0.99	1.00	1.03	0.99	1.05	0.68
Total	100.01	99.53	100.00	99.31	99.93	99.21	99.14	99.99	99.98
A/CNK	1.00	1.12	1.02	1.04	1.05	1.05	1.07	1.19	1.02
					Trace (ppm)				
Sc	9.94	1.69	14.7	6.56	6.11	4.06	9.41	24.2	11.5
V	12.2	8.54	4.78	3.26	17.1	12.4	2.03	2.44	3.12
Cr	7.84	5.59	5.82	4.12	8.15	7.95	3.68	6.60	7.45
Ni	2.37	1.40	1.12	1.58	3.53	2.72	1.98	1.37	1.56
Ga	25.8	26.2	23.8	22.9	19.4	19.6	23.0	24.7	23.1
Rb	270	318	466	427	162	185	490	408	390
Sr	27.9	20.7	2.76	7.04	104	99.3	7.79	6.69	8.02
Y	65.4	79.6	50.4	78.6	30.1	26.6	66.9	104.6	77.4
Zr	266	246	191	159	298	232	126	143	130
Nb	49.4	50.5	33.3	32.0	29.1	21.5	28.6	33.6	30.5
Cs	2.29	7.08	15.8	16.4	3.70	12.5	14.2	13.4	15.0
Ba	158	153	3.94	8.05	978	1071	20.7	22.4	27.8
La	56.4	62.6	43.5	47.6	68.5	71.1	62.9	127	68.0
Ce	116	127	76.7	98.9	137	141	136	86	147
Pr	12.3	13.2	10.0	11.5	14.3	14.2	14.7	31.8	16.3
Nd	45.1	48.2	37.4	44.1	53.9	51.7	55.6	123	61.6
Sm	10.5	11.3	9.30	11.4	9.92	8.82	13.0	29.1	14.4
Eu	0.50	0.51	0.10	0.16	1.76	1.69	0.19	0.28	0.18
Gd	9.69	10.9	8.41	11.5	7.21	5.94	11.4	22.4	12.6
Tb	1.80	2.10	1.53	2.06	1.13	0.97	2.05	3.83	2.33
Dy	11.4	13.4	9.36	12.7	6.24	5.29	12.2	21.3	14.2
Ho	2.33	2.80	1.84	2.55	1.16	1.01	2.39	3.93	2.81
Er	6.92	8.21	5.32	7.32	3.21	2.82	6.79	10.8	8.09
Tm	1.04	1.25	0.80	1.10	0.45	0.41	0.99	1.53	1.18
Yb	6.76	7.74	5.06	6.87	2.84	2.57	6.06	9.36	7.36
Lu	0.98	1.13	0.73	0.98	0.42	0.40	0.86	1.32	1.06
Hf	10.2	9.28	8.65	6.88	8.65	7.08	5.64	6.99	6.19
Ta	4.80	4.26	4.32	3.42	1.93	1.64	3.38	4.19	3.59
Pb	26.6	31.5	50.7	37.1	25.7	27.7	42.6	23.3	44.9
Th	35.8	40.0	25.9	38.2	21.9	24.0	42.4	49.1	45.5
U	7.87	9.28	11.6	9.34	4.32	5.68	12.7	9.07	14.2

Table continues

TABLE 4. *Continued*

Sample	2KGN34-8	2KGN34-12	2KGN16-1	2KGN16-3	2KGN16-5	2KGN16-7	2KGN16-9	2KGN16-10	2KGN16-11
					Major (%)				
SiO_2	74.74	76.67	67.65	65.20	61.95	67.82	62.21	65.69	60.79
TiO_2	0.11	0.09	0.22	0.37	0.52	0.24	0.50	0.41	0.58
Al_2O_3	13.02	11.46	16.13	16.10	17.42	15.13	16.06	16.43	17.37
Fe_2O_3	1.81	1.64	3.27	4.79	4.96	3.41	5.57	2.98	5.02
MnO	0.02	0.02	0.08	0.17	0.16	0.09	0.20	0.18	0.18
MgO	0.06	0.04	0.12	0.43	0.55	0.14	0.53	0.11	0.37
CaO	0.48	0.41	0.95	1.22	1.37	0.88	1.98	0.95	1.86
Na_2O	3.25	2.86	5.62	5.37	6.05	5.42	5.51	4.64	5.65
K_2O	5.81	5.03	5.35	5.94	6.03	5.40	5.57	5.99	6.18
P_2O_5	0.02	0.01	0.03	0.08	0.10	0.03	0.09	0.04	0.12
LOI	0.61	1.02	0.55	0.84	1.06	0.87	1.57	1.78	1.65
Total	99.94	99.25	99.97	100.53	100.16	99.42	99.79	99.21	99.76
A/CNK	1.04	1.05	0.96	0.92	0.92	0.92	0.86	1.04	0.90
					Trace (ppm)				
Sc	10.1	9.29	6.17	6.95	6.43	3.73	5.24	6.21	8.33
V	1.18	2.55	1.32	0.33	0.79	0.67	0.30	1.44	1.20
Cr	6.34	6.32	3.28	4.37	3.44	2.64	4.63	1.27	3.82
Ni	1.07	1.60	1.33	0.88	0.77	1.46	1.18	0.84	0.70
Ga	23.4	21.9	24.8	22.0	21.8	25.8	20.6	24.3	21.4
Rb	380	366	126	97.5	80.2	138	89.1	137	85.3
Sr	6.85	6.78	48.1	48.6	46.6	25.9	46.1	47.6	58.0
Y	74.2	70.4	42.6	21.0	19.3	51.9	20.7	42.3	21.0
Zr	128	129	313	146	340	462	251	693	242
Nb	32.8	25.8	71.8	31.9	33.7	88.4	38	52.7	44.8
Cs	12.9	12.4	5.75	17.5	3.10	6.93	4.86	3.88	2.84
Ba	18.6	18.3	826	1173	1293	222	1238	367	1394
La	69.0	65.9	54.8	41.8	23.7	78.5	26.5	38.5	31.8
Ce	147	140	109	82.3	51.0	158	56.3	86.1	68.3
Pr	16.4	15.6	11.7	8.81	6.07	16.37	6.63	10.0	7.89
Nd	61.5	58.7	43.5	33.0	24.8	60.5	26.6	39.9	31.8
Sm	14.6	13.8	9.00	6.14	5.09	12.1	5.45	8.63	6.34
Eu	0.20	0.19	1.59	2.46	2.72	1.10	2.69	1.81	3.07
Gd	12.5	12.1	7.65	4.60	4.27	10.1	4.61	7.67	5.06
Tb	2.29	2.19	1.46	0.80	0.73	1.83	0.78	1.41	0.85
Dy	13.6	13.1	7.88	4.12	3.76	9.86	4	7.79	4.31
Ho	2.70	2.57	1.60	0.79	0.77	1.93	0.79	1.57	0.83
Er	7.60	7.22	4.70	2.27	2.19	5.44	2.26	4.67	2.30
Tm	1.13	1.04	0.69	0.33	0.34	0.82	0.34	0.72	0.34
Yb	7.07	6.42	4.32	2.14	2.26	5.10	2.26	4.75	2.20
Lu	1.00	0.93	0.63	0.34	0.38	0.76	0.37	0.75	0.35
Hf	6.03	5.87	9.65	4.54	6.96	12.5	5.96	14.1	5.64
Ta	3.60	2.84	5.04	2.07	2.06	5.82	2.46	3.77	2.85
Pb	39.1	39.4	16.3	13.6	7.75	14.3	12.7	12.9	7.60
Th	44.5	42.0	12.4	5.53	2.27	15.0	3.43	9.70	2.84
U	10.2	8.16	3.21	1.18	0.96	2.83	1.15	2.67	0.79

Table continues

TABLE 4. *Continued*

Sample	2KGN18-1	2KGN18-4	2KGN18-5	2KGN22-1	2KGN22-2	2KGN22-3	2KGN22-4	2KGN22-5	2KGN22-6
					Major (%)				
SiO_2	65.91	68.03	66.58	67.26	67.88	67.10	67.28	65.98	66.76
TiO_2	0.62	0.65	0.68	0.48	0.50	0.50	0.48	0.50	0.48
Al_2O_3	13.79	14.31	14.25	14.46	14.51	13.98	14.59	14.92	14.51
Fe_2O_3	4.13	4.65	5.35	5.57	5.53	5.69	5.54	5.51	5.57
MnO	0.05	0.04	0.08	0.15	0.15	0.17	0.15	0.14	0.14
MgO	0.78	0.78	0.91	0.16	0.18	0.17	0.16	0.17	0.16
CaO	3.24	0.99	1.40	0.99	0.84	0.95	0.81	1.10	1.03
Na_2O	3.79	4.25	4.40	5.40	5.27	5.22	5.22	5.86	5.65
K_2O	4.79	4.66	4.24	5.13	5.27	4.97	5.26	5.10	5.08
P_2O_5	0.16	0.18	0.18	0.11	0.10	0.11	0.10	0.12	0.11
LOI	3.22	1.47	1.87	0.57	0.71	0.52	0.59	0.57	0.49
Total	100.47	100.01	99.95	100.27	100.93	99.38	100.18	99.96	99.97
ACNK	0.80	1.03	0.99	0.89	0.91	0.89	0.93	0.87	0.87
					Trace (ppm)				
Sc	5.22	10.1	5.28	0.51	8.75	0.32	0.59	6.99	4.11
V	27.6	33.1	31.8	1.45	1.94	2.29	2.10	1.29	1.55
Cr	5.02	4.99	3.50	5.92	5.10	6.70	4.98	4.30	8.39
Ni	1.86	1.84	1.99	0.98	0.88	1.02	0.79	1.04	1.21
Ga	20.1	21.8	21.6	31.3	32.2	31.7	32.8	32.1	32.2
Rb	234	221	184	83.8	82.5	84.1	83.9	83.2	84.2
Sr	173	163	189	45.3	41.0	41.7	38.8	52.3	39.7
Y	30.4	32.9	27.8	39.4	30.2	51.2	39.7	83.9	66.5
Zr	248	276	279	239	307	241	252	278	295
Nb	37.5	42.0	42.4	52.9	57.2	52.4	53.6	55.0	56.2
Cs	9.10	9.92	7.48	2.52	2.63	2.68	2.76	0.69	0.70
Ba	827	696	642	793	776	755	725	1011	947
La	34.4	54.8	46.0	90.7	82.5	103	100	143	134
Ce	69.8	109	90.6	151	153	161	152	207	203
Pr	7.53	11.5	9.34	20.7	18.0	22.9	22.3	31.7	29.6
Nd	28.5	43.1	34.4	79.6	66.4	89.5	84.3	126	114
Sm	6.20	8.67	6.82	15.2	12.2	17.2	16.0	25.1	23.1
Eu	1.29	1.79	1.24	3.64	2.76	4.19	3.70	5.60	4.67
Gd	5.46	6.89	5.61	11.0	7.82	13.7	11.6	19.4	16.8
Tb	1.01	1.22	1.00	1.84	1.41	2.28	1.93	3.25	2.82
Dy	5.54	6.31	5.24	8.87	6.83	11.1	9.23	15.9	13.6
Ho	1.12	1.20	1.04	1.59	1.28	2.03	1.64	2.93	2.52
Er	3.37	3.44	3.02	4.18	3.60	5.27	4.35	7.73	6.70
Tm	0.53	0.51	0.46	0.57	0.52	0.69	0.59	1.03	0.91
Yb	3.44	3.32	3.06	3.64	3.38	4.16	3.71	6.36	5.64
Lu	0.52	0.50	0.46	0.55	0.53	0.63	0.57	0.94	0.85
Hf	7.12	7.98	7.93	6.23	8.05	6.32	6.63	7.48	7.79
Ta	3.36	3.76	3.73	3.13	3.66	3.14	3.22	3.59	3.75
Pb	11.6	65.6	156	5.09	6.25	5.21	5.20	4.89	5.07
Th	18.4	20.8	21.3	8.80	11.8	8.70	9.30	10.5	10.7
U	7.65	9.58	8.98	1.39	2.07	1.37	1.45	1.75	1.80

A/CNK = molecular $Al_2O_3/(Na_2O + K_2O + CaO)$; Total iron as Fe_2O_3.

TABLE 5. Sr-Nd isotopic data

Sample	Sm (ppm)	Nd (ppm)	$^{147}Sm/^{144}Nd$	$^{143}Nd/^{144}Nd \pm 2\sigma_m$	εNd(T)	Rb (ppm)	Sr (ppm)	$^{87}Rb/^{86}Sr$	$^{87}Sr/^{86}Sr \pm 2\sigma_m$	$(^{87}Sr/^{86}Sr)_i$
Chebu gabbro										
2KGN29-1	4.60	18.6	0.1495	0.512613 ±0.000010	0.55	65.1	267	0.705	0.708413 ±0.000018	0.7067
2KGN29-4	4.10	17.0	0.1458	0.512567 ±0.000013	–0.27	58.7	264	0.643	0.708105 ±0.000017	0.7065
2KGN29-5	4.84	20.4	0.1434	0.512537 ±0.000012	–0.82	52.5	263	0.577	0.707955 ±0.000014	0.7066
Zhaibei granite										
2KGN28-1	10.5	45.1	0.1407	0.512536 ±0.000010	–0.78	270	27.9	28.0		
2KGN28-6	11.3	48.2	0.1417	0.512526 ±0.000010	–1.00	318	20.7	44.4		
2KGN31-3	9.92	53.9	0.1113	0.512325 ±0.000008	–4.27	162	104	4.50	0.721989 ±0.000013	0.7110
2KGN34-5	29.1	123	0.1430	0.512243 ±0.000009	–6.55	408	6.69	176		
2KGN34-7	14.4	61.6	0.1413	0.512241 ±0.000010	–6.55	390	8.02	141		
2KGN34-8	14.6	61.5	0.1435	0.512291 ±0.000011	–5.61	380	6.85	160		
Quannan syenite										
2KGN16-1	9.00	43.5	0.1251	0.512618 ±0.000006	1.08	126	48.1	7.57	0.723552 ±0.000020	0.7061
2KGN16-3	6.14	33.0	0.1125	0.512687 ±0.000006	2.69	97.5	48.6	5.80	0.718889 ±0.000035	0.7056
2KGN16-5	5.09	24.8	0.1241	0.512734 ±0.000007	3.37	80.2	46.6	4.98	0.717849 ±0.000010	0.7064
2KGN16-7	12.1	60.5	0.1209	0.512611 ±0.000005	1.04	138	25.9	15.4	0.745800 ±0.000015	0.7103
2KGN16-9	5.45	26.6	0.1239	0.512720 ±0.000006	3.10					
2KGN16-10	8.63	39.9	0.1307	0.512643 ±0.000006	1.45	137	47.6	8.32	0.723849 ±0.000017	0.7048
2KGN16-11	6.34	31.8	0.1205	0.512734 ±0.000007	3.44	85.3	58.0	4.25	0.716893 ±0.000013	0.7071
2KGN18-1	6.20	28.5	0.1315	0.512387 ±0.000005	–3.54	234	173	3.91	0.718497 ±0.000010	0.7095
2KGN18-4	8.67	43.1	0.1216	0.512384 ±0.000005	–3.41	221	163	3.92	0.718614 ±0.000016	0.7097
2KGN18-5	6.82	34.4	0.1198	0.512396 ±0.000006	–3.15	184	189	2.81	0.715806 ±0.000011	0.7094
Tabei seynite										
2KGN22-2	12.2	66.4	0.1111	0.512581 ±0.000008	0.65	82.5	41.0	5.82	0.718298 ±0.000016	0.7049
2KGN22-5	25.1	126	0.1204	0.512580 ±0.000009	0.42	83.2	52.3	4.60	0.714651 ±0.000016	0.7041
2KGN22-6	23.1	114	0.1225	0.512559 ±0.000009	–0.02	84.2	39.7	6.13	0.718323 ±0.000016	0.7043

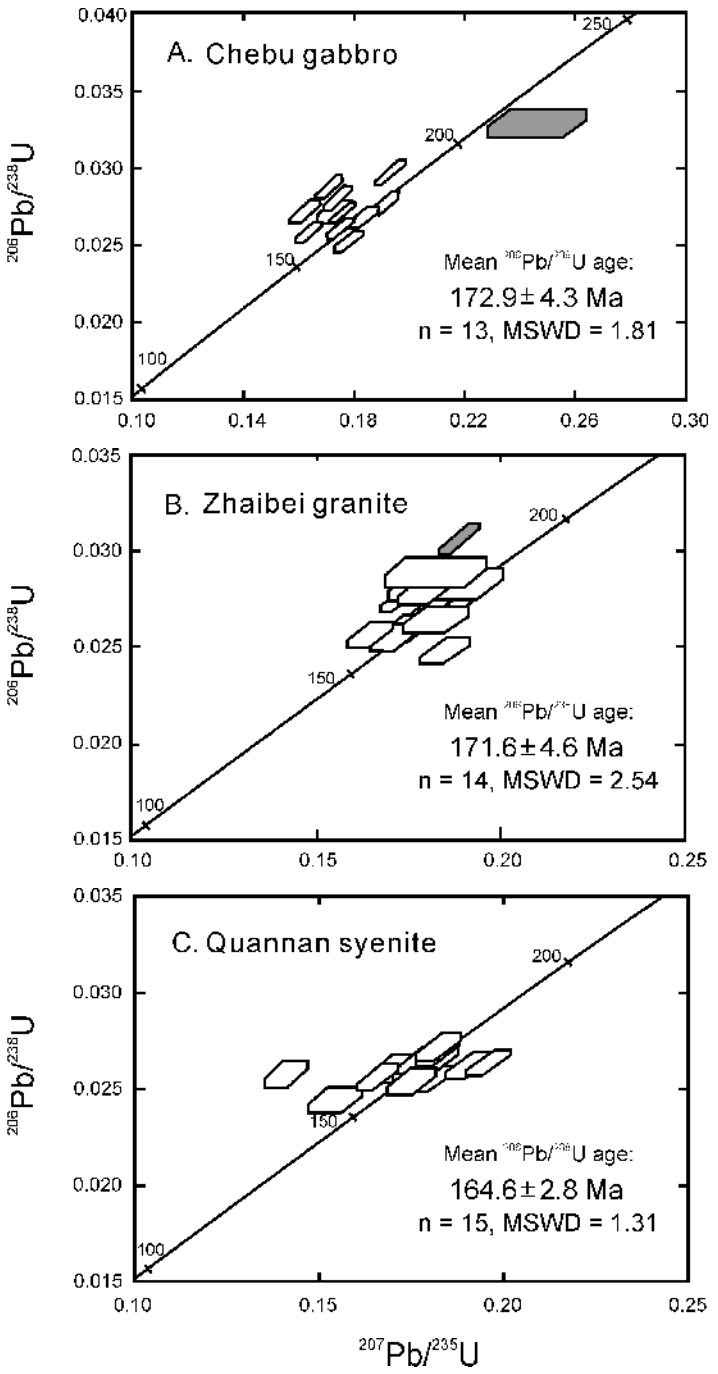

FIG. 3. U-Pb concordia diagrams showing analytical data for zircons from (A) the Chebu gabbro, (B) the Zhaibei granite, and (C) the Quannan syenite.

group, form a single, concordant group, yielding a weighted mean $^{206}Pb/^{238}U$ age of 171.6 ± 4.6 Ma (MSWD = 2.54, Fig. 3B). This age is interpreted as the crystallization age of the Zhaibei granite.

The Quannan syenite (sample 2KGN16-1, 24°46'20.4" N, 114°29'55.7" E). Zircons are mostly euhedral, range up to 200 μm in length, and have length-to-width ratios up to 3:1. Most crystals are transparent and colorless. Euhedral concentric zoning is common; no inherited zircon cores were observed. Fifteen analyses were conducted of 15 zircons in sets of seven scans. Concentrations of U range from 255 to 1635 ppm, and Th from 227 to 852 ppm. Th/U ratios vary between 0.54 and 1.34.

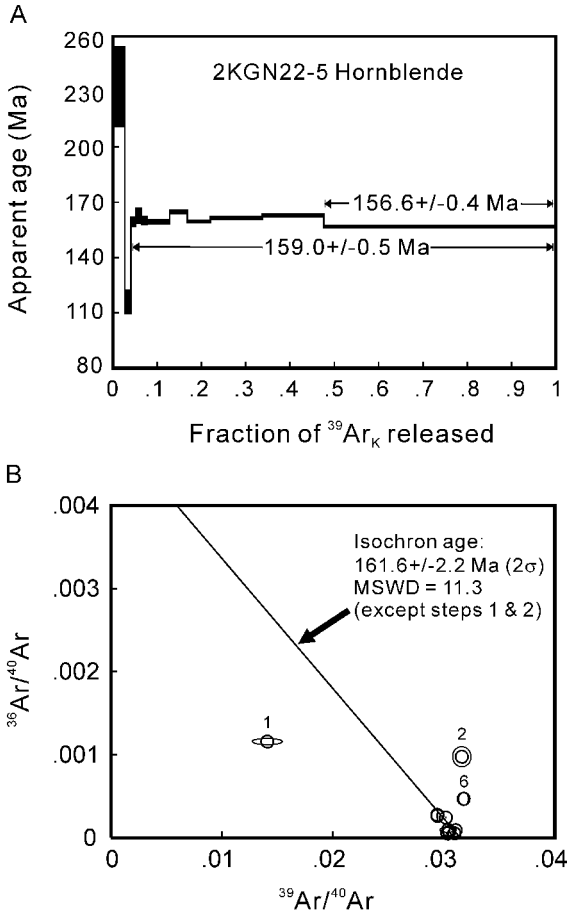

FIG. 4. $^{40}Ar/^{39}Ar$ age spectra (A) and $^{39}Ar/^{40}Ar$–$^{36}Ar/^{40}Ar$ inversion isochron diagrams (B) for hornblende from the Tabei syenite. The length of steps represents the relative volume of ^{39}Ar released, and the height of the solid rectangles indicates the 1σ relative uncertainties.

All analyses form a single, concordant group in $^{206}Pb/^{238}U$ ratios corresponding to a weighted mean $^{206}Pb/^{238}U$ age of 164.6 ± 2.8 Ma (Fig. 3C), which is considered as the best estimate of the crystallization age of the Quannan syenite.

Hornblende $^{40}Ar/^{39}Ar$ date

The Tabei syenite (sample 2KGN22-5, 24°57'59.1" N, 114°44'14.3" E). The hornblende $^{40}Ar/^{39}Ar$ results are plotted as the age spectrum and inversion isochron diagrams in Figure 4. The $^{40}Ar/^{39}Ar$ age spectrum diagram demonstrates that a plateau age cannot be obtained from the analytical results. Although steps 3 to 10 at 950–1250°C gi ve apparent $^{40}Ar/^{39}Ar$ dates ranging from 159.0 ± 0.8 Ma (1ó) to 165.1 ± 0.6 Ma (1σ), the last step at 1600°C yields a lower apparent date of 156.6 ± 0.2 Ma (1σ) with 52.4% accumulated ^{39}Ar. On the inversion isochron plot, most data points are close to the $^{39}Ar/^{40}Ar$ axis due to high radiogenic ^{40}Ar (very low $^{36}Ar/^{40}Ar$ ratio). Apart from analyses of the first two steps at low temperatures (= 900 °C), the remaining analyses of steps 3 to 11 yield an isochron age of 161.6 ± 2.2 Ma (2σ), indistinguishable within error from the total integrated age of 159.0 ± 0.5 Ma (2σ). The isochron age of 161.6 ± 2.2 Ma is thus interpreted as the cooling age of Tabei syenite at ~550°C (hornblende Ar blocking temperature), which is consistent within error with the U-Pb zircon age of the Quannan syenite, and thus should be very close to the crystallization age of the Tabei syenite. In summary, the SHRIMP U-Pb zircon and hornblende $^{40}Ar/^{39}Ar$ dating results document two main episodes of Jurassic plutonism in southern Jiangxi: the bimodal gabbro-granite intrusion at ~172 Ma and the syenite intrusion at ~165 Ma.

Geochemistry

Chebu gabbro samples have a restricted range of SiO_2 (48.8%–51.3%) and consistent total alkali contents ($Na_2O + K_2O$ = 3.8–4.2%). On the TAS rock classification diagram (Fig. 5A), they plot on the subalkaline gabbro side near the boundary between the subalkalic and alkalic fields. They are relatively high in Al_2O_3 (15.7–16.8%), but lower in TiO_2 (1.2–1.5%) and P_2O_5 (~0.2%) compared to those of the typical intraplate basaltic rocks (TiO_2 > 2%, P_2O_5 > 0.3%) (Wilson, 1989). On the other hand, their major-element compositions are also different from those of the basaltic rocks from island arcs (Al_2O_3 <16%, TiO_2 <1%, P_2O_5 <0.3%) and active continental margins (Al_2O_3 >17%, TiO_2 <1.2%, P_2O_5 <0.4%) (Wilson, 1989). These gabbro samples have a relatively high Nb/Y ratio (0.62–0.67), an index of alkalinity, intermediate between subalkaline and alkaline basaltic rocks (Fig. 5B). Taken together, the Chebu gabbro displays transitional geochemical features between subalkaline and alkaline basaltic rocks. The gabbro samples have uniform REE patterns (Fig. 6A), showing moderate LREE enrichment with La_N = 68–85, $(La/Yb)_N$ = 5.1–5.8, and moderate to negligible negative Eu anomalies (Eu/Eu* = 0.75–0.99) On a primitive mantle-normalized spidegram (Fig. 7A), the Chebu gabbros show increasing enrichment in immobile incompatible elements from Lu to Th with increasing incompatibility, apart from a weak depletion in Nb and Ta (Nb/La = 0.79–0.94).

The Zhaibei granite samples are highly siliceous (SiO_2 = 71.1–76.7%) and peraluminous with A/CNK

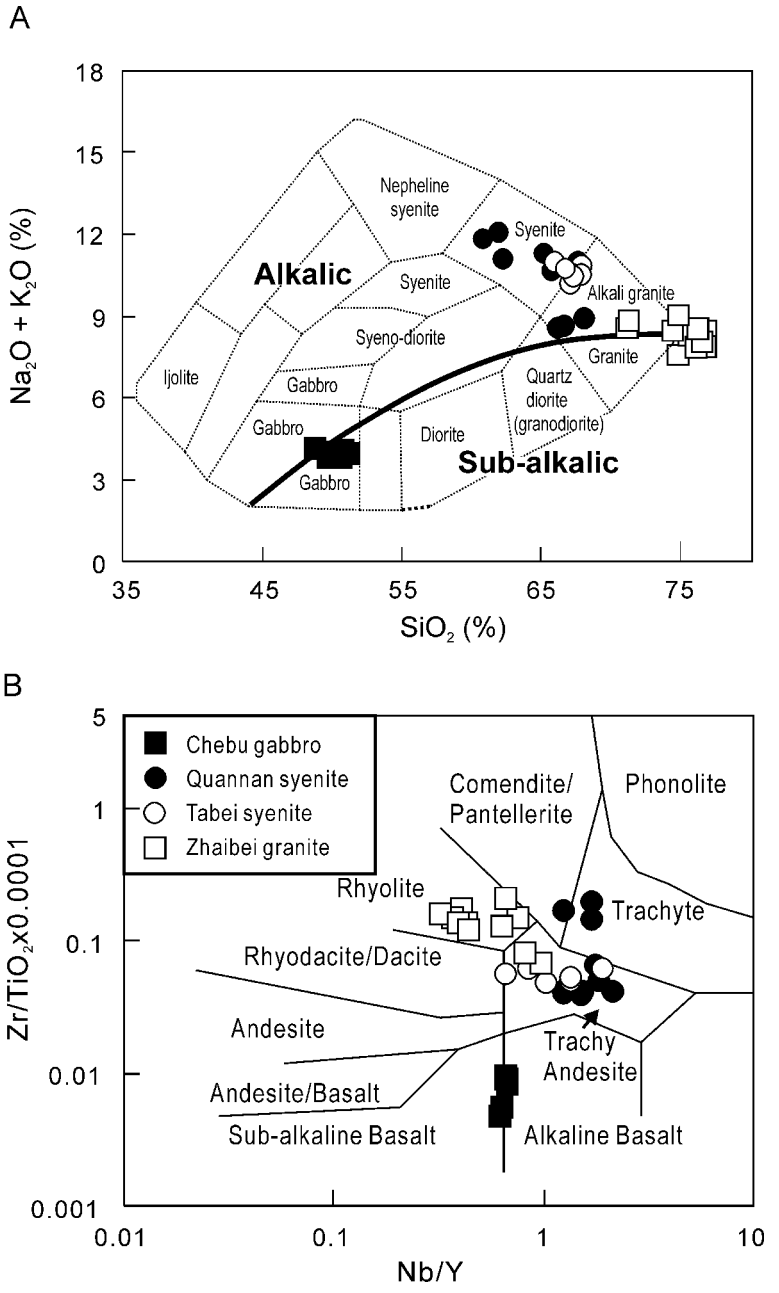

FIG. 5. Rock classification diagrams of (A) SiO_2 vs. $K_2O + Na_2O$ (Cox et al., 1979), and (B) Nb/Y vs. Zr/TiO_2 (Winchester and Floyd, 1977). Analyzed samples are shown.

values clustering mostly around 1.0–1.1. They are rich in alkalis with K_2O = 4.8–5.8% and Na_2O = 2.5–3.7%, mostly plotting into the alkaline granite field close to the boundary between the subalkalic and alkalic fields on the TAS diagram (Fig. 5A). They are low in total Fe_2O_3 (1.6–3.7%), MnO (<0.05%), MgO (0.04–0.27%), CaO (0.15–1.1%), TiO_2 (0.09–0.44%), and P_2O_5 (< 0.1%), but are highly enriched in LREE (Fig. 6B), with La_N = 179–519, $(La/Yb)_N$ = 4.7–18.7, and extremely negative Eu anomalies (Eu/Eu* = 0.03–0.15) except for the two least felsic samples, 2KGN31-3 and 2KGN 33-1, which show moderate negative Eu anomalies (Eu/Eu* = 0.6–0.7). They are variably high in Ga, Rb, Zr, Nb, REE, and Y, and low in Ba and Sr. On a spidergram (Fig. 7B), all granitic rocks show characteristic negative anomalies in Nb, Ta, Sr, P, Eu, and Ti relative to the neighboring elements. In general, the Zhaibei granites share features with A-type granites in terms of major- and trace-element geochemistry (Collins et al., 1982; Whalen et al., 1987). Their

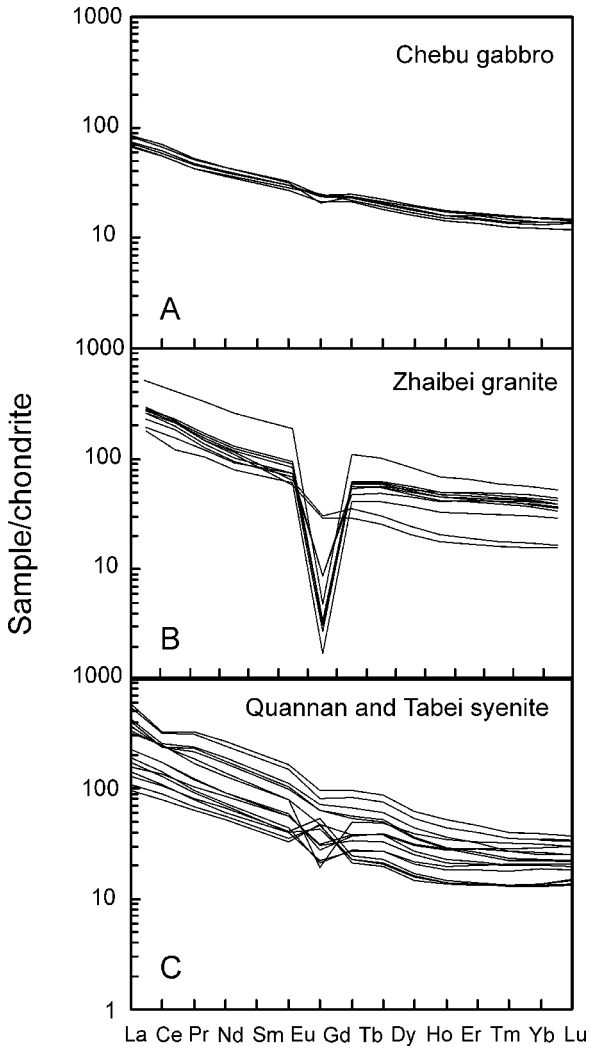

FIG. 6. Chondrite-normalized REE diagrams for (A) the Chebu gabbro, (B) the Zhaibei granite, and (C) Quannan and Tabei syenites. Normalization values are from Sun and McDonough (1989).

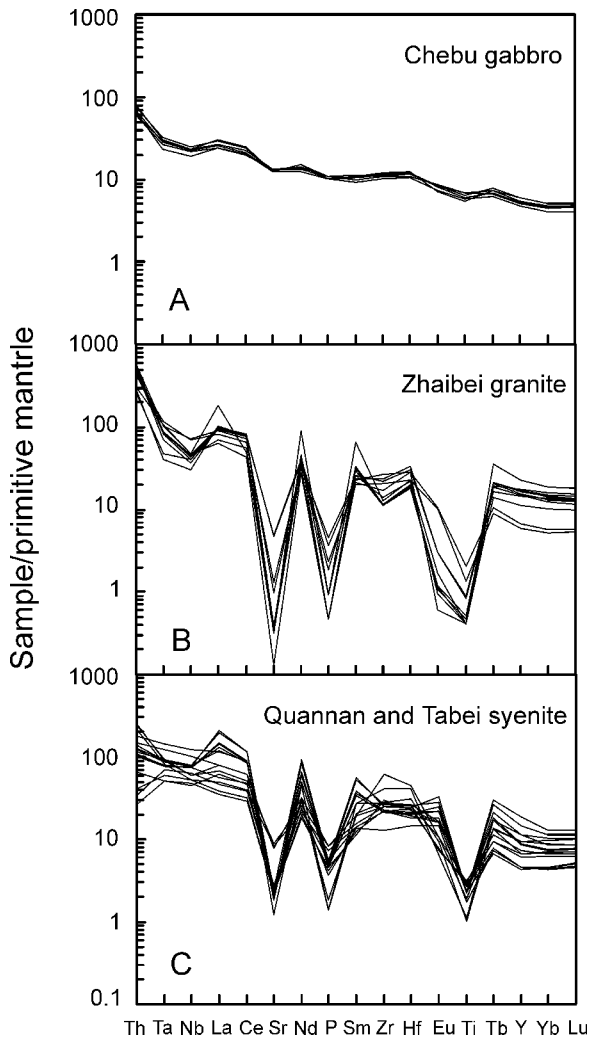

FIG. 7. Primitive mantle–normalized incompatible-element spidergrams for (A) the Chebu gabbro, (B) the Zhaibei granite, and (C) the Quannan and Tabei syenites. Normalization values are from Sun and McDonough (1989).

10,000 × Ga/Al ratios range from 2.7 to 4.0, with an average value of 3.5, which is slightly lower than the global average of 3.75 for A-type granites (Whalen et al., 1987), but are comparable to the aluminous A-type granites in Northeast China (Fig. 8; Wu et al., 2002).

The Quannan and Tabei syenites show relatively restricted SiO_2 contents of 60.8–67.9% and high alkalis ($K_2O + Na_2O$ = 8.6–12.1%). They have very low MgO (<1%), indicating extreme crystal fractionation. On the TAS diagram, they mostly fall into the syenite field, with a few samples falling into the alkali granite field (Fig. 5A). They are characterized by high Nb/Y ratios (0.66–2.13) , typical of alkaline igneous rocks (Fig. 5B). All syenite samples are high in K_2O with K_2O/Na_2O ratios of 0.9–1.3, showing shoshonitic affinity. They display variable LREE-enriched patterns with La_N = 97–421, $(La/Yb)_N$ = 5.5–18.2, and variable degrees of a negative Eu anomaly (Eu/Eu* = 0.3–0.8), except for a few of the least felsic samples from Quannan that have positive Eu anomalies (Eu/Eu* = 1.4–1.7). On the spidergram (Fig. 6C), the syenites are characterized by variable enrichment in all trace elements, with the exception of Sr, P, and Ti that show varying degrees of negative anomaly due to intensive crystal fractionation. The southern Jiangxi syenites have no evident Nb-Ta depletion relative to La, contrasting with most potassic alkaline rocks occurring in arc-related settings (e.g., Müller and Groves, 1995).

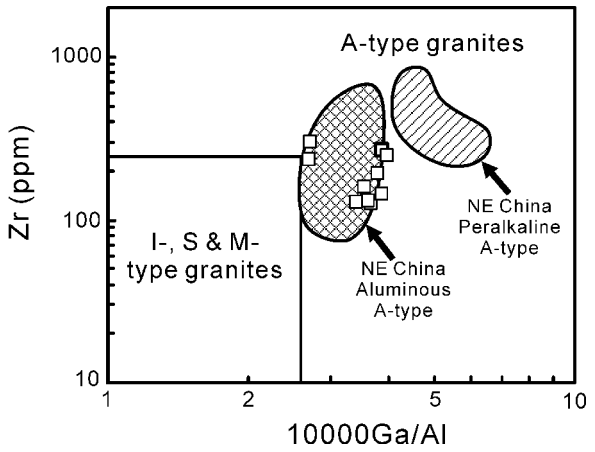

FIG. 8. Zr vs. 10000*Ga/Al diagram of Whalen et al. (1987) for the Zhaibei granite, which is similar to the aluminous A-type granites in Northeast China (Wu et al., 2002). Analyzed Zhaibei samples indicated.

Most Quannan samples have high Nb/La ratios of 1.1–1.4, resembling many alkali basalts formed in oceanic islands and continental rift areas (Sun and McDonough, 1989).

Sr-Nd isotopes

Three Chebu gabbro samples have a restricted range of Sr and Nd isotopic compositions, with initial $^{87}Sr/^{86}Sr$ ratios (I_{Sr}) of 0.7065 to 0.7067 and εNd(T) values of +0.55 to –0.82. In contrast, six Zhaibei granite samples have a wide range of εNd(T) values, from –0.78 to –6.55. Among the analyzed granites, two samples (2KGN28-1 and 2KGN28-6) collected near the Chebu gabbro have the highest εNd(T) values of –0.78 to –1.0, probably due to interaction between the felsic and mafic magmas as shown by the described petrographic features. We analyzed the Sr isotopic composition of one granite sample (2KGN31-3), the least felsic Zhaibei granite with the lowest $^{87}Rb/^{86}Sr$ ratio of 4.50. This sample has I_{Sr} = 0.7110, significantly higher than that of the Chebu gabbro. Other highly fractionated granite samples were not analyzed for Sr isotopes, because they have very high $^{87}Rb/^{86}Sr$ ratios of 28–176 that will cause large uncertainties in the calculated I_{Sr} by correction of radiogenic ^{87}Sr (Wu et al., 2002). The Quannan syenites have variable Nd and Sr isotopic compositions with εNd(T) values of –3.54 to +3.44 and I_{Sr} of 0.7048–0.7103, whereas, the Tabei syenites show restricted Nd and Sr isotopic compositions with εNd(T) values = –0.02 to +0.65 and I_{Sr} = 0.7041–0.7049.

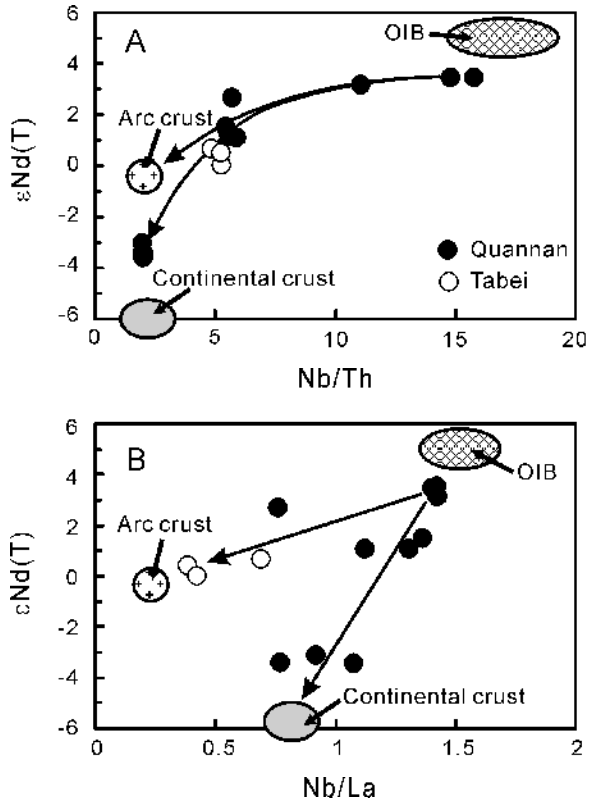

FIG. 9. εNd(T) values vs. Nb/Th and Nb/La diagrams for the Quannan and Tabei syenites. Analyzed rocks shown.

The I_{Sr} ratios are not negatively correlated with εNd(T) values, possibly caused by redistribution of Rb and Sr during subsequent alteration. On the other hand, the εNd(T) values are positively correlated with Nb/Th ratios for the syenites (Fig. 9A). Samples 2KGN16-5 and 2KGN16-11 with the highest εNd(T) value ≈ +3.4 have the highest Nb/Th ratios of 15–16, comparable with Nb/Th = 14–20 for oceanic island basalts (Sun and McDonough, 1989). Thus, the parental magma of the syenites might have been generated from an enriched mantle source with εNd(T) ≈ +4 at ~165 Ma. Their εNd(T) values are also positively correlated with Nb/La ratios, forming two binary mixing trends towards continental and arc crusts (Fig. 9B).

Discussion

Petrogenesis

As described above, the Chebu gabbros have major- and trace-element geochemical characteristics significantly different from those of volcanic arc basalts, as shown by totally different trace-element patterns (Fig. 10A). Although most of the gabbros

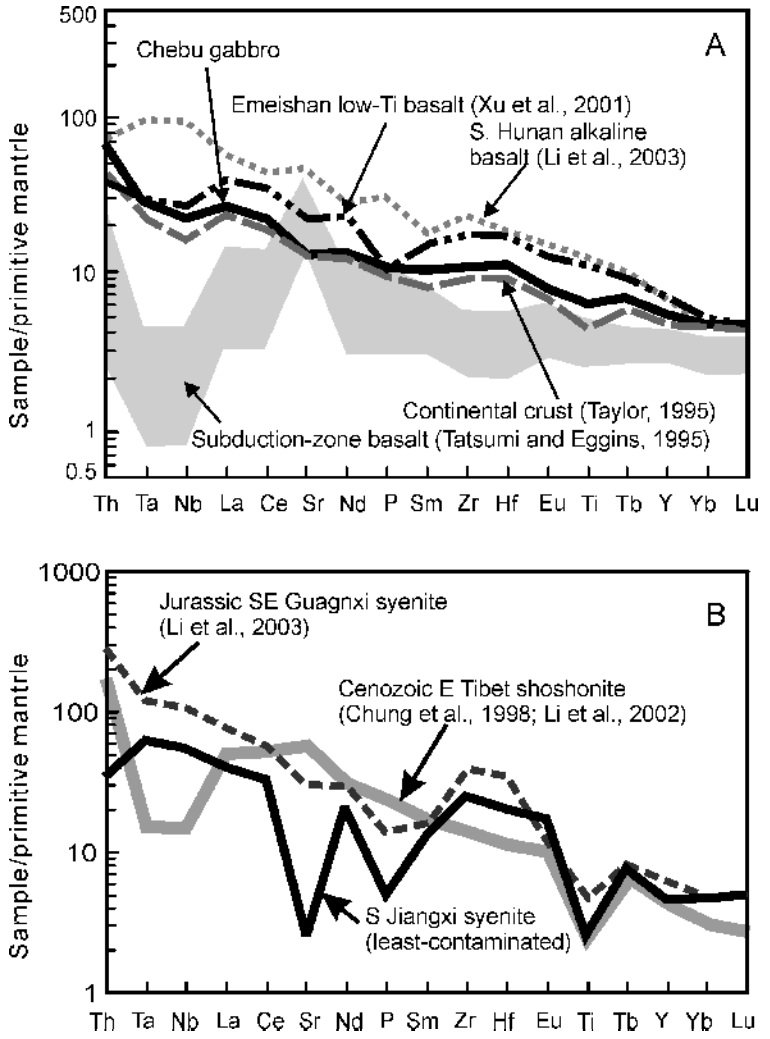

FIG. 10. A. Incompatible-element spidergrams showing comparison between the Chebu gabbro (this study) and the Emeishan low-Ti basalts (Xu et al., 2001), southern Hunan alkaline basalts (Li et al., 2003), continental crust (Taylor and McLennan, 1995) and subduction-zone basalts (Tatsumi and Eggins, 1995). B. Incompatible-element spidergrams showing comparison between the least contaminated Quannan syenites and the Southeast Guangxi syenites (Li et al., 2003) and Southeast Tibetan potassic alkaline rocks (Chung et al., 1998; Li et al., 2002b).

display generally "humped" trace-element spidergrams similar to those of intraplate basalts, they have lower abundance in most incompatible trace elements (except Th) than the latest Permian Emeishan low-Ti transitional basalt of predominant lithosphere mantle origin (Xu et al., 2001) and the ~175 Ma alkaline basalts of possible asthenospheric origin in southern Hunan (Li et al., 2003). They show geochemical affinities with intraplate basalts, but with superimposed crustal signatures such as weak Nb-Ta negative anomalies and incompatible-trace-element abundances between those of typical intraplate basalts and continental crust. Such transitional geochemical features also can be seen in certain discrimination diagrams. For instance, on the Ti-Zr-Y diagram of Pearce and Cann (1973), the gabbros straddle the boundary between within-plate and volcanic arc basalts (Fig. 11A), whereas, on the Y-La-Nb ternary plot of Cabanis and Lecolle (1989), the gabbros plot exclusively into the field of continental basalts (Fig. 11B). The εNd(T) values, which correlate positively with Nb/La and Nb/Th ratios, also suggest continental and/or arc crustal contamination in the origin of the Chebu gabbro.

The question is whether the contamination occurred during mafic intrusion into the crust, or if the mantle source itself had been previously contaminated. There are two types of mantle source contamination, or mantle metasomatism: (1) subduction-related metasomatized mantle source

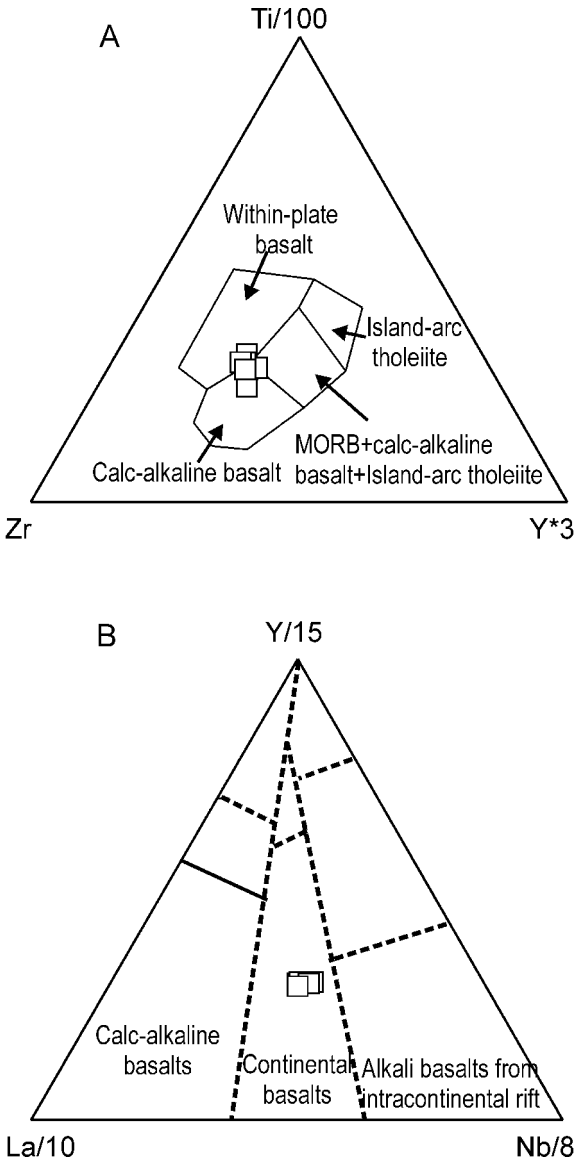

FIG. 11. A. Ti-Zr-Y discrimination diagram of Pearce and Cann (1973). B. La-Y-Nb discrimination diagram of Cabanis and Lecolle (1989). Samples of analyzed Chebu gabbro indicated.

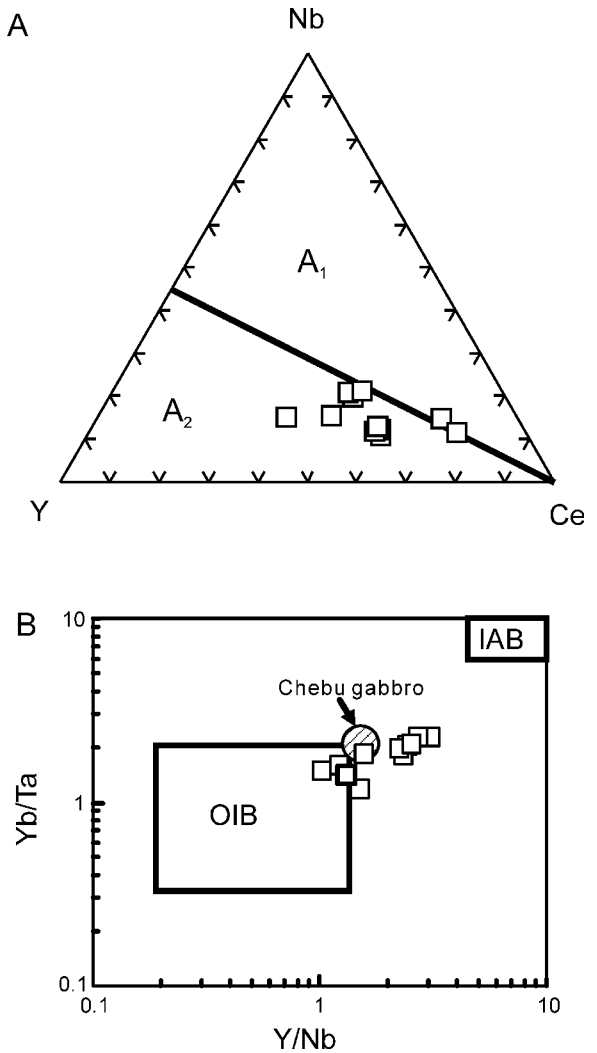

FIG. 12. Plots of the Zhaibei granites in (A) the Nb-Y-Ga ternary diagrams for a subdivision of the A_1-and A_2-type granites, and (B) the Yb/Ta vs. Y/Nb diagram of Eby (1992).

enriched in LILE and LREE but depleted in HFS elements; and (2) asthenosphere-derived melt-metasomatized mantle, which is enriched in LILE, LREE, and HFS elements. Subduction-related metasomatism is characterized by significant depletion of HFS elements with very low HFS/LREE ratios (Nb/La ratio usually <0.3), contrasting to the metasomatism of asthenosphere-derived melt. Thus, basaltic rocks derived from subduction-related metasomatized mantle typically show significant Nb-Ta anomalies. In contrast, basaltic rocks derived from mantle metasomatized by asthenosphere-derived melt usually have high HFS/LREE ratios (Nb/La ratio >1). The Chebu gabbro samples have an Nb/La ratio of 0.79–0.94, which is significantly higher than those of the basaltic rocks in subduction- and/or arc-related settings (such as continental arc, oceanic arc, and post-collisional arc environments). Therefore, a subduction-related metasomatized mantle source was not likely for the origin of the Chebu gabbro. Instead, the parental magma of the gabbro was probably derived from an enriched lithospheric mantle metasomatized by an OIB-type melt very shortly before the generation of basaltic magmas. The process was accompanied by crustal contaminations during fractional crystallization of the magma, indicated by the generally "humped" incompatible trace-element spidergrams (Fig. 10A)

and relatively high Nb/La and Nb/Y ratios in the gabbro samples.

According to the geochemical subdivision by Eby (1992), the Zhaibei granite belongs to the A_2-type granites on the Nb-Y-Ce triangular plot (Fig. 12A). They have Yb/Ta = 1.2–2.3 and Y/Nb = 1.0–3.1, generally higher than those of OIB, with a few samples having low Yb/Ta and Y/Nb ratios overlapping the OIB field and the Chebu gabbro (Fig. 12B).

Although the Zhaibei A-type granite could have been produced by extreme differentiation of basaltic parent magmas (e.g., Turner et al., 1992; Bonin, 1996), this is not likely for several reasons. First, the volume of A-type felsic rocks in southern Jiangxi is large compared with the mafic rocks. Second, there is a "Daly gap" between mafic and felsic rocks. Third, the distinct Nd isotopic compositions are not consistent with a simple magma differentiation model. Two granite samples have Nd isotopes similar to the Chebu gabbro, due possibly to chemical interaction of the mafic and felsic magmas as mentioned above.

Melting experiments indicate that dehydration melting of hornblende-bearing granitoids at a pressure < 4 kbar is likely responsible for the origin for high-silica A-type granites (Patiño Douce, 1997). A-type magmas are usually generated in non-compressive tectonic regimes such as extension or rifting environments, where the crust tends to be thin and magmatic advection of heat can approach shallow levels of the crust. Such a model seems appropriate for generation of the Zhaibei A-type granite. Attaining the required melting temperature (>900°C) at relatively shallow levels of the crust requires heat and/or mass transfer from mantle-derived, hot basaltic magmas during the production of the A-type granites; the contemporaneous basalts and gabbros in southern Jiangxi might have been acted as such heat source.

The Quannan and Tabei syenites exhibit variable trace element and Nd isotopic compositions, with a few samples having εNd values > +3 and OIB-like trace-element patterns. It has been generally considered that potassic alkaline magmas are generated by small-degree melting of a metasomatized mantle source modified either by subduction-derived fluids/melts enriched in LILE and LREE but depleted in HSFE, or by an asthenosphere-derived melt with OIB-type geochemical features. Müller and Groves (1995) classified potassic alkaline igneous rocks into two main categories: (1) the majority of potassic alkaline rocks formed in various subduction- or arc-related settings ("arc-type"), such as continental arc, oceanic arc, and post-collisional arc environments; and (2) others occurring within continental and oceanic settings ("intraplate type") including those affiliated with rifts and hotspots, such as the potassic rocks from the Navajo province (Roden, 1981) and the western branch of the East African Rift (Thompson et al., 1984; Rogers et al., 1998). The Quannan syenite samples have an incompatible trace-element pattern (Fig. 10B) significantly different from the majority of "arc-type" potassic rocks, such as those from southeastern Tibet (Chung et al., 1998; Li et al., 2002b), with pronounced Nb-Ta negative anomalies (Nb/La < 0.3). They display a general trace-element pattern lacking an Nb-Ta negative anomaly (Nb/La >1) (with the exception of significant troughs in Sr, P, and Ti, which may be due to fractional crystallization), similar to the Jurassic "intraplate-type" syenites in Southeast Guangxi (Li et al., 2003). Hence, the parental magma of the syenites was probably derived from an enriched lithospheric mantle source that had been metasomatized, shortly before the generation of potassic magmas, by an OIB-type melt. Some Quannan samples have negative εNd values and a small negative Nb-Ta anomaly, indicative of involvement of continental crustal materials (Fig. 9B). In contrast, the Tabei syenites have a restricted range of εNd values (–0.02 to 0.65) and a pronounced negative Nb-Ta anomaly (Nb/La = 0.4–0.7), possibly due to variable involvement of arc components.

Tectonic implications

As mentioned above, the tectonic regime that accounted for the Mesozoic (particularly the early Mesozoic) magmatism in Southeast China has been an issue of long-term debate. Hsü et al. (1988, 1990) proposed an Alpine-type continental collision model for the Mesozoic tectonics of Southeast China—i.e., that the Huanan block collided with the Yangtze craton during the Triassic, and then with the postulated Dongnanya block during Tria-Jurassic to Cretaceous time. In their collision model, the Neoproterozoic Banxi Group on the Yangtze side was re-interpreted as a Mesozoic mélange and a far-traveled thrust sheet, and the Cretaceous granites in Southeast China as the products of collision between the Huanan block and the Dongnanya microcontinents. However, this collision model has been refuted by many studies since it was proposed (e.g., Rodgers 1989; Rowley *et al.* 1989; Chen *et al.* 1991; Li and McCulloch, 1996). For instance, many recent

investigations have demonstrated that the Banxi Group and overlying Sinian System are normal sedimentary sequences (e.g., Li and McCulloch, 1996; Wang and Li, 2001, 2003), which formed within the Neoproterozoic Nanhua Rift basin related to the initial rifting of the supercontinent Rodinia (Li et al., 1999; Wang and Li, 2003). U-Pb zircon dating and geochemical results (Li et al., 1995; Zou, 1995) indicate that the Quanzhou gabbro in coastal Fujian Province crystallized within the continent at 107 Ma, rather than representing an ophiolitic member of the "Quanzhou Klippe" proposed by Hsü et al. (1990).

Eastern China was characterized by a series of large-scale, NE-trending fault systems, such as the Tancheng-Lujiang and Changle-Nanao shear zones along the coastal regions of northeastern and southeastern China, respectively; these were collectively named as the Tancheng-Lujiang wrench fault system by Xu et al. (1987, 1993). These authors inferred that the oceanic plate might have not been subducted beneath the East Asian continent until Late Cretaceous time; the Mesozoic Yanshanian granites in Southeast China were considered as the products of faulting-induced re-melting. While the faulting-induced re-melting explains the formation of the syntectonic, deformed granites along the Changle-Nanao shear zone (Tong and Tobisch, 1996; Yui et al., 1996), it seems not to be applicable to the widespread Mesozoic Yanshanian granites in Southeast China, inasmuch as the majority of granites are neither deformed nor associated with fractures.

An active continental margin related to subduction of the paleo-Pacific plate is favored by many authors for development of calc-alkaline volcanic and intrusive rocks during the Jurassic to Cretaceous in the coastal region of Southeast China (e.g., Jahn et al., 1976, 1990; Huang et al., 1986; Charvet et al., 1994; Martin et al., 1994; Lan et al., 1996; Lapierre et al., 1997; Sewell and Campbell, 1997). The subduction-related regime was considered to be dominant until the Late Cretaceous when alkaline granites formed along the Fujian coast (e.g. Charvet et al., 1994; Martin et al., 1994). Recently, a modified subduction model was proposed by Zhou and Li (2000) to account for the exceptionally wide magmatic arc and the migration of magmatic activity oceanward to the southeast. They suggested an increase of slab dip of the paleo-Pacific plate subduction underneath Southeast China from a very low angle in Early Jurassic to a median one in Late Cretaceous time. However, such a subduction model, which rests mainly on the prevailing arc signatures observed in the Cretaceous igneous rocks, is inconsistent with continental extension and rifting in Southeast China (Gilder et al., 1991, 1996; Li, 2000; Li et al., 2000, 2003). A system of Mesozoic NE-trending grabens in Southeast China was considered as an analogy to the present-day Basin and Range Province in the western United States—i.e., "Southeast China Basin and Range Province" (Gilder et al., 1991). Upper Triassic–Cretaceous extensional basins, such as the Shiwandashan Basin in Southeast Guangxi (Gilder et al., 1996), mostly developed on Paleozoic to Middle Triassic basement that was ubiquitously folded during the Indosinian Orogeny (Li, 1998). Thus, the extension and rifting probably commenced in the Late Triassic–Early Jurassic. During this period of extension and rifting, the ~175 Ma alkaline basalts and ~160 Ma syenites with OIB-like geochemical and isotopic features (Nb/La >1, I_{Sr} = 0.703–0.704 and εNd(T) = +5 to +6) formed in southern Hunan and southeastern Guangxi (Li et al., 2000, 2003), ~300 km west to southern Jiangxi. The association of A-type granitic and intraplate basaltic magmatism of 140–90 Ma also supports an extension to rift regime in Southeast China during most of Cretaceous time, and the arc signatures in the igneous rocks were considered as inheritance from pre-existing arc source materials (Li, 2000). The two early episodes of Cretaceous intraplate magmatism during 140–120 Ma correspond to the timing of the final doming of possible core complexes in Wugongshan, Lushan, and Jiulingshan (Faure et al., 1996; Lin et al., 2000, 2001).

Our new geochronological, geochemical, and Sr-Nd isotopic data for the gabbro-granite-syenite suites in southern Jiangxi shed new light on the Mesozoic tectonics of Southeast China. First, there is a general consensus that A-type granites are mostly emplaced in extensional or non-compressional tectonic settings (Whalen et al., 1987; Sylvester, 1989; Rogers and Greenberg, 1990; Eby, 1990, 1992), which might be related to different tectonic settings, such as anorogenic rifts, lithospheric extension, and late- to post-orogenic gravitational collapse. The coeval A-type felsic and mafic magmatism in southern Jiangxi suggests that the regional extensional crustal thinning was closely related in time and space to deep-seated thermal activity due to mantle-derived mafic magma influx. In addition, the ~175 Ma alkaline basalts in southern Hunan (Li et al., 2003) and the ~172 Ma bimodal magmatic association (Chen et al., 1999;

this study) provide support for an intraplate extension and/or rift setting origin, rather than an arc environment in which calc-alkaline, intermediate rocks are dominant.

Second, the ~165 Ma syenites in southeastern Guangxi (Li et al., 2000, 2003) and southern Jiangxi (this study) are of typical "intraplate-type" potassic alkaline rocks, which were derived from an enriched lithospheric mantle that had been metasomatized by an OIB-type melt very shortly before magma generation. In southern Hunan, the ~175 Ma alkaline basalts likely were responsible for this kind of mantle metasomatism (Li et al., 2003). Such mantle metasomatism by OIB-type melts usually occurs in an intraplate environment, in contrast to the metasomatized mantle wedge over a subduction zone by fluids and melts released from the subducting slab. Thus, an active continental margin characterized by low-angle subduction is unlikely.

Third, the occurrence of alkaline basalts and bimodal volcanic/plutonic rocks and intraplate-type syenites in southern Hunan–southeastern Guangxi and southern Jiangxi suggests an extension-to-rifting regime prevalent over much of the Southeast China interior during Middle to Late Jurassic time. Southeast China probably was a rifted continental margin during this period.

Conclusions

SHRIMP U-Pb zircon and hornblende $^{40}Ar/^{39}Ar$ age determinations document two major episodes of Jurassic magmatism in southern Jiangxi, represented by~172 Ma bimodal mafic and A-type felsic rocks and~165 Ma syenite in southern Jiangxi. The bimodal intrusive/extrusive and syenite suites were emplaced over a wide area of Southeast China during the Middle to Late Jurassic (~175–160 Ma). These igneous rocks display geochemical and Sr-Nd isotopic affinities of intraplate, extension-, and/or rift-related magmatism. Large-scale mantle metasomatism by subduction-derived fluids/melts, which usually take place in the mantle wedge over a subduction zone, was not observed in the interior of Southeast China. Therefore, an active continental margin typified by low-angle subduction was not likely. Instead, a rifted continental margin seems appropriate to account for the Middle to Late Jurassic magmatism in Southeast China.

Acknowledgments

We thank S. L. Chung and J. H. Yang for assistance in $^{40}Ar/^{39}Ar$ dating, P. Jian in SHRIMP U-Pb analysis, Y. Liu and X. L. Tu in major- and trace-element analysis, and X. Liang in Sr-Nd isotope analyses. J.-X. Zhao is thanked for proofreading the paper. This work was supported by the Chinese Academy of Sciences (grant KZCX2-102) and National Science Foundation of China (NSFC grant 49725309).

REFERENCES

Bonin, B., 1996, A-type granite ring complex: mantle origin through crustal filters and the anorthosite-rapakivi magmatism connection, *in* Demaiffe, D., ed., Petrology and geochemistry of magmatic suites of rocks in the continental and oceanic crusts: Brussels, Belgium, Université Libre de Bruxelles, Royal Museum for Central Africa (Tervuren), p. 201–218.

Cabanis, B., and Lecolle,. M., 1989, Le diagramme La/10-Y/15-Nb/8: un outil pour la discrimination des series volcaniques et la mise en evidence des procesus de melange et/ou de contamination crutale: Comptes Rendus de'l Academie des Sciences, ser. II, v. 309, p. 2023–2029.

Charvet, J., Lapierre, H., and Yu, Y., 1994, Geodynamic significance of the Mesozoic volcanism of southeastern China: Journal of Southeast Asian Earth Sciences, v. 68, p. 387–396.

Chen, J. F., Foland, K. A., Xing, F., Xu, X., and Zhou, T. X., 1991, Magmatism along the southeast margin of the Yangtze block: Precambrian collision of the Yangtze and Cathaysia blocks of China: Geology, v. 19, p. 815–818.

Chen, P. R., Kong, X. G., Wang, Y. X., Ni, Q. S., Zhang, B. T., and Ling, H. F., 1999, Rb-Sr isotopic dating and significance of early Yangshanian bimodal volcanic-intrusive complex from southern Jiangxi Province, SE China: Geological Journal of China Universities, v. 5, p. 378–382 (in Chinese with English abstract).

Chung, S. L., Lo, C. H., Lee, T. Y., Zhang, Y., Xie, Y., Li, X. H., Wang, K. L., and Wang, P. L., 1998, Diachronous uplift of the Tibetan plateau staring 40 Myr ago: Nature, v. 394, p. 769–773.

Collins, W. J., Beams, S. D., White, A. J. R., and Chappell, B. W., 1982, Nature and origin of A-type granites with particular reference to southeastern Australia: Contributions to Mineralogy and Petrology, v. 80, p. 189–200.

Cox, K. G., Bell, J. D., and Pankhurst, R. J., 1979, The interpretation of igneous rocks. London, UK: Allen and Unwin, 450 p.

Cumming, G. L., and Richards, J. R., 1975, Ore lead isotope ratios in a continuously changing Earth: Earth and Planetary Science Letters, v. 28, p. 155–171.

Eby, G. N., 1990, The A-type granitoids: A review of their occurrence and chemical characteristics and speculations on their petrogenesis: Lithos, v. 26, p. 115–134.

_____, 1992, Chemical subdivision of the A-type granitoids: Petrologic and tectonic implications: Geology, v. 20, p. 641–644.

Fan, C. F., and Chen, P. R., 2000, Geochemical characteristics and tectonic implication of Pitou A-type granitic intrusive in South Jiangxi province: Geochimica, v. 29, p. 358–366 (in Chinese with English abstract).

Faure, M., Sun, Y., Shu, L., Monié, P., and Charvet, J., 1996, Extensional tectonics within a subduction-type orogen: The case study of the Wugongshan dome (Jiangxi Province, SE China): Tectonophysics, v. 263, p. 77–108.

Gilder, S. A., Gill, J., Coe, R. S., Zhao, X. X., Liu, Z., Wang, G., Yuan, K., Liu, W., Kuang, G., and Wu, H., 1996, Isotopic and paleomagnetic constraints on the Mesozoic tectonic evolution of south China: Journal of Geophysical Research, v. 101(B7), p. 16,137–16,154.

Gilder, S. A., Keller, G. R., Luo, M., and Goodell, P. C., 1991, Timing and spatial distribution of rifting in China: Tectonophysics, v. 197, p. 225–243.

Holloway, N. H., 1982, North Palawan Block, Philippines—its relation to Asian mainland and role in evolution of South China Sea: American Association of Petroleum Geologists Bulletin, v. 66, p. 1355–1383.

Hsü, K. J., Li, J. L., Chen, H. H., Pen, H. P., and Sengor, A. M. C., 1990, Tectonics of south China: Key to understanding west Pacific geology: Tectonophysics, v. 183, p. 9–39.

Hsü, K. J., Sun, S., Li, J. L., Chen, H. H., Pen, H. P., and Sengor, A. M. C., 1988, Mesozoic overthrust tectonics in south China: Geology, v. 16, p. 418–421.

Huang, X., Sun, S. H., DePaolo, D. J., and Wu, K. L., 1986, Nd-Sr isotope study of Cretaceous magmatic rocks from Fujian province: Acta Petrologica Sinica, v. 2, p. 28–36 (in Chinese with English abstract).

Jahn, B. M., Chen, P. Y., and Yen, T. P., 1976, Rb-Sr ages of granitic rocks in southeastern China and their tectonic significance: Geological Society of America Bulletin, v. 86, p. 763–776.

Jahn, B. M., Zhou, X. H., and Li, J. L., 1990, Formation and tectonic evolution of southeast China: Isotopic and geochemical constraints: Tectonophysics, v. 183, p. 145–160.

JBGMR (Jiangxi Bureau of Geology and Mineral Resources), 1989, Regional geology of Hunan Province: Beijing, China, Geological Publishing House, 504 p. (in Chinese).

Lan, C. Y., Jahn, B. M., Mertzman, S. A., and Wu, T. W., 1996, Subduction-related granitic rocks of Taiwan: Journal of Southeast Asian Earth Sciences, v. 14, p. 11–28.

Lapierre, H., Jahn, B. M., Charvet, J., and Yu, Y. W., 1997, Mesozoic magmatism in Zhejiang Province and its relation with the tectonic activities in SE China: Tectonophysics, v. 274, p. 321–338.

Li, H. M., Dong, C. W., Xu, X. S., and Zhou, X. M., 1995, U-Pb single-grain zircon dating of the Quanzhou Gabbro: Implications for the origin of basic magmatism in SE Fujian: Chinese Science Bulletin, v. 40, p. 158–160 (in Chinese).

Li, X. H., 1997, Geochemistry of the Longsheng ophiolite from the southern margin of Yangtze Craton, SE China: Geochemical Journal, v. 31, p. 323–337.

_____, 2000, Cretaceous magmatism and lithospheric extension in Southeast China: Journal of Asian Earth Sciences, v. 18, p. 293-305.

Li, X. H., Chung, S. L., Zhou, H. W., Lo, C. H., Liu, Y., and Chen, C. H., 2003, Jurassic intraplate magmatism in southern Hunan–eastern Guangxi: $^{40}Ar/^{39}Ar$ dating, geochemistry, Sr-Nd isotopes, and implications for tectonic evolution of SE China, *in* Malpas, J., Fletcher, C., and Ali, J. R., eds., Tectonic processes in the evolution of China: Geological Society of London Special Publication, in press.

Li, X. H., Liu, Y., Tu, X., Hu, G., and Zeng, W., 2002a, Precise determination of chemical compositions in silicate rocks using ICP-AES and ICP-MS: A comparative study of sample digestion techniques of alkali fusion and acid dissolution: Geochimica, v. 31, p. 289–294 (in Chinese with English abstract).

Li, X. H. and McCulloch, M. T., 1996, Secular variations in the Nd isotopic composition of Late Proterozoic sediments from the southern margin of the Yangtze Block: Evidence for a Proterozoic continental collision in SE China: Precambrian Research, v. 76, p. 67–76.

Li, X. H., Zhou, H., Chung, S. L., Lo, C. H., Wei, G., Liu, Y., and Lee, C. Y., 2002b, Geochemical and Sr-Nd isotopic characteristics of late Paleogene ultrapotassic mgamatism in southeastern Tibet: International Geology Review, v. 44, p. 559–574.

Li, X. H., Zhou, H., Liu, Y., Lee C.-Y., Sun, M., and Chen, C. H., 2000, Shoshonitic intrusive suite in SE Guangxi: Petrology and geochronology: Chinese Science Bulletin, v. 45, p. 653–658.

Li, Z. X., 1998, Tectonic evolution of the major East Asian lithospheric blocks since mid-Proterozoic—a synthesis, *in* Martin, F. J., Chung, S.-L., Lo, C.-H., and Lee, T.-Y., eds., Mantle dynamics and plate interactions in East Asia: Washington, DC, American Geophysical Union, p. 221–243.

Li, Z. X., Li, X. H., Kinny, P. D., and Wang, J., 1999, The breakup of Rodinia: Did it start with a mantle plume beneath South China?: Earth Planetary and Science Letters, v. 173, p. 171–181.

Liang, X. R., Wei, G. J., Li, X. H., and Liu, Y., 2003, Precise determination of $^{143}Nd/^{144}Nd$ and Sm/Nd ratios using multiple-collector inductively coupled plasma-

mass spectrometer (MC-ICPMS): Geochimica, v. 32, p. 91–96 (in Chinese with English abstract).

Lin, W., Faure, M., Monié, P., Schärer, U., Zhang, L., and Sun, Y., 2000, Tectonic of SE China: New insights from the Lushan massif (Jiangxi Province): Tectonics, v. 19, p. 852–871.

Lin, W., Faure, M., Sun, Y., Sun, L., and Wang, Q., 2001, Compression to extension switch during the middle Triassic orogeny in eastern China: The case study of the Jiulingshan massif in the southern foreland of the Dabieshan: Journal of Asian Earth Sciences, v. 20, p. 31–43.

Liu, Y., Liu, H. C., and Li, X. H., 1996, Simultaneous and precise determination of 40 trace elements in rock samples by ICP-MS: Geochimica, v. 25, p. 552–558 (in Chinese with English abstract).

Lo, C. H., and Lee, C. Y., 1994, $^{40}Ar/^{39}Ar$ method of K-Ar age determination of geological samples using the Tsing-Hua Open-Pool Reactor (THOR): Journal of the Geological Society of China, v. 37, p. 143–164.

Martin, H., Bonin, B., Capdevila, R., Jahn, B. M., Lameyre, J., and Wang, Y., 1994, The Kuiqi peralkaline granitic complex (SE China): Petrology and geochemistry: Journal of Petrology, v. 35, p. 983–1015.

Müller, D., and Groves, D., 1995, Potassic igneous rocks and associated gold-copper mineralization: Berlin, Germany, Springer-Verlag, 144 p.

Odin, G. S., and 35 collaborators, 1982, Interlaboratory standards for dating purposes, *in* Odin, G. S., ed., Numerical dating in stratigraphy: Chichester, UK, Wiley, p. 123–149.

Patiño Douce, A. E., 1997, Generation of metaluminous A-type granites by low-pressure melting of calc-alkaline granitoids: Geology, v. 25, p. 743–746.

Pearce, J. A., and Cann, J. R., 1973, Tectonic setting of basic volcanic rocks determined using trace element analyses: Earth and Planetary Science Letters, v. 19, p. 290–300.

Roden, M. F., 1981, Origin of coexisting minette and ultramafic breccia, Navajo volcanic field: Contributions to Mineralogy and Petrology, v. 77, p. 195–206.

Rodgers, J., 1989, Comment on "Mesozoic overthrust tectonics in south China": Geology, v. 17, p. 671–672.

Rogers, J. J. W., and Greenberg, J. E., 1990, Late-orogenic, postorogenic, and anorogenic granites: Distinction by major-element and trace-element chemistry and possible origins: Journal of Geology, v. 98, p. 291–310.

Rogers, N. W., James, D., Kelley, S. P., and De Mulder, M., 1998, The generation of potassic lavas from the eastern Virunga province, Rwanda: Journal of Petrology, v. 39, p. 1223–1247.

Rowley, D. B., Ziegler, A. M., and Gyou, N., 1989, Comment on "Mesozoic overthrust tectonics in south China": Geology, v. 17, p. 384–386.

Sewell, R. J., and Campbell, S. D. G., 1997, Geochemistry of coeval Mesozoic plutonic and volcanic suites in Hong Kong: Journal of the Geological Society of London, v. 154, p. 1053–1066.

Song, B., Zhang, Y., Wan, Y., and Jian, P., 2002, Mount making and procedure of the SHRIMP dating: Geological Review, v. 48 (suppl.), p. 26–30 (in Chinese with English abstract).

Sun, S.-S., and McDonough, W. F., 1989, Chemical and isotopic systematics of oceanic basalt: Implications for mantle composition and processes, *in* Saunders, A. D., and Norry, M. J., eds., Magmatism in the ocean basins: Geological Society of London Special Publication, 42, p. 528–548.

Sylvester, P. J., 1989, Post-collisional alkaline granites: Journal of Geology, v. 97, p. 261–280.

Tanaka, T., and 19 co-authors, 2000, JNdi-1: A neodymium isotopic reference in consistency with La Jolla neodymium: Chemical Geology, v. 168, p. 279–281.

Tatsumi, Y., and Eggins, S. M., 1995, Subduction zone magmatism: Cambridge, UK and Boston, MA, Blackwell Scientific, 211 p.

Taylor, S. R., and McLennan, S. M., 1995, The geochemical evolution of the continental crust: Reviews of Geophysics, v. 32, p. 241–265.

Thompson, R. N., Morison, M. A., Hendry, G. L., and Parry, S. J., 1984, An assessment of the relative roles of crust and mantle in magma genesis: An element approach: Philosophical Transactions of the Royal Society of London, v. A310, p. 549–590.

Tong, W. X., and Tobisch, O. T., 1996, Deformation of granitoid plutons in the Dongshan area, southeast China: Constraints on the physical conditions and timing of movement along the Changle-Nanao shear zone: Tectonophysics, v. 267, p. 303–316.

Turner, S. P., Foden, J. D., and Morrison, R. S., 1992, Derivation of some A-type magmas by fractionation of basaltic magma: An example from the Padthaway Ridge, South Australia: Lithos, v. 28, p. 151–179.

Vernon, R. H., Etheridge, M. A., and Wall, V. J., 1988, Shape and microstructure of microgranitoids enclaves: Indicators of magma mingling and flow: Lithos, v. 22, p. 1–11.

Wang, J., and Li, Z. X., 2001, Sequence stratigraphy and evolution of the Neoproterozoic marginal basins along southeastern Yangtze Craton, South China: Gondwana Research, v. 4, p. 17–26.

_____, 2003, History of Neoproterozoic rift basins in South China: Implications for Rodinia breakup: Precambrian Research, v. 122, p. 141–158.

Wei, G. J., Liang, X. R., Li, X. H., and Liu, Y., 2002, Precise measurement of Sr isotopic composition of liquid and solid base using (LP)MC-ICPMS: Geochimica, v. 31, p. 35–42 (in Chinese with English abstract).

Whalen, J. B., Currie, K. L., and Chappell, B. W., 1987, A-type granites: Geochemical characteristics, discrimination and petrogenesis: Contributions to Mineralogy and Petrology, v. 95, p. 407–419.

Williams, I. S., 1998, U-Th-Pb geochronology by ion microprobe, *in* McKibben, M. A., Shanks, W. C., and Ridley, W. I., eds., Applications of microanalytical techniques to understanding mineralizing processes: Reviews of Economic Geology, v. 7, p. 1–35.

Wilson, M. 1989, Igneous petrogenesis: London, UK, Unwin Hyman, 466 p.

Winchester, J. A., and Floyd, P. A., 1977, Geochemical discrimination of different magma series and their differentiation products using immobile elements: Chemical Geology, v. 20, p. 325–343.

Wu, F. Y., Sun, D. Y., Li, H. M., Jahn, B. M., and Wilde, S. A., 2002, A-type granites in Northeastern China: Age and geochemical constraints on their petrogenesis: Chemical Geology, v. 187, p. 143–173.

Xu, J., Ma, G., Tong, W. X., Zhu, G., and Lin, S., 1993, Displacement of the Tancheng-Lujiang wrench fault system and its geodynamic setting in the northwestern Circum-Pacific, *in* Xu, J., ed., The Tancheng Lujiang wrench fault system: New York, NY, John Wiley & Sons, p. 51–74.

Xu, J., Zhu, G., Tong, W. X., Gui, K. R., and Liu, Q., 1987, Formation and evolution of the Tancheng-Lujiang wrench fault system: A major shear system to the northwest of the Pacific Ocean: Tectonophysics, v. 134, p. 273–310.

Xu, X., Dong, C., Li, W., and Zhou, X., 1999, Late Mesozoic intrusive complexes in the coastal area of Fujian, SE China: The significance of the gabbro-diorite-granite association: Lithos, v. 46, p. 299–315.

Xu, Y., Chung, S. L., Jahn, B. M., and Wu, G., 2001, Petrologic and geochemical constraints on the petrogenesis of Permian–Triassic Emeishan flood basalts in southwestern China: Lithos, v. 58, p. 145–168.

Yui, T. F., Heaman, L., and Lan, C. Y., 1996, U-Pb and Sr isotopic studies on granitoids from Taiwan and Chinmen-Lieyu and their tectonic implications: Tectonophysics, v. 263, p. 61–76.

Zhou, X. M., and Li, W. X., 2000, Origin of Late Mesozoic igneous rocks in Southeastern China: Implications for lithosphere subduction and underplating of mafic magmas: Tectonophysics, v. 326, p. 269–287.

Zou, H. B., 1995, A mafic-ultramafic rock belt in the Fujian coastal area, southeastern China: A geochemical study: Journal of Southeast Asia Earth Sciences, v. 12, p. 121–127.